

Systems-level effects of allosteric perturbations to a model molecular switch

<https://doi.org/10.1038/s41586-021-03982-6>

Received: 1 January 2020

Accepted: 1 September 2021

Published online: 13 October 2021

 Check for updates

Tina Perica^{1,2,3,12}, Christopher J. P. Mathy^{1,2,4,12}, Jiewei Xu^{2,5,6}, Gwendolyn M. Jang^{2,5,6}, Yang Zhang^{1,2}, Robyn Kaake^{2,5,6}, Noah Ollikainen^{1,2,7}, Hannes Braberg^{2,5,6}, Danielle L. Swaney^{2,5,6}, David G. Lambright^{8,9}, Mark J. S. Kelly¹⁰, Nevan J. Krogan^{2,5,6} & Tanja Kortemme^{1,2,4,7,11}

Molecular switch proteins whose cycling between states is controlled by opposing regulators^{1,2} are central to biological signal transduction. As switch proteins function within highly connected interaction networks³, the fundamental question arises of how functional specificity is achieved when different processes share common regulators. Here we show that functional specificity of the small GTPase switch protein Gsp1 in *Saccharomyces cerevisiae* (the homologue of the human protein RAN)⁴ is linked to differential sensitivity of biological processes to different kinetics of the Gsp1 (RAN) switch cycle. We make 55 targeted point mutations to individual protein interaction interfaces of Gsp1 (RAN) and show through quantitative genetic⁵ and physical interaction mapping that Gsp1 (RAN) interface perturbations have widespread cellular consequences. Contrary to expectation, the cellular effects of the interface mutations group by their biophysical effects on kinetic parameters of the GTPase switch cycle and not by the targeted interfaces. Instead, we show that interface mutations allosterically tune the GTPase cycle kinetics. These results suggest a model in which protein partner binding, or post-translational modifications at distal sites, could act as allosteric regulators of GTPase switching. Similar mechanisms may underlie regulation by other GTPases, and other biological switches. Furthermore, our integrative platform to determine the quantitative consequences of molecular perturbations may help to explain the effects of disease mutations that target central molecular switches.

Proteins perform their cellular functions within networks of interactions with many partners³. The interconnectivity of these networks raises the fundamental question of how different individual functions can be controlled with the required specificity, especially when distinct cellular processes share common regulators. Moreover, in highly interconnected networks even small perturbations could have widespread cellular effects^{6,7}.

To determine the mechanism and extent by which molecular perturbations affect interconnected biological processes, we targeted a central molecular switch—a GTPase. GTPases are two-state switches controlled by regulators with opposing functions². The two states of GTPase switches are defined by the conformation of their GTP- or GDP-bound forms, and the interconversion between states is catalysed by guanine nucleotide exchange factors (GEFs) and GTPase-activating proteins (GAPs) (Fig. 1a). Other, similar biological switch motifs involve covalent modifications controlled by opposing kinase–phosphatase or acetylase–deacetylase regulators. One notable feature of such motifs is

their potential for ultrasensitive response to regulation, whereby small changes in the activity of the regulators can lead to sharp changes in the state of the switch^{1,2}. Moreover, switch motifs such as GTPases are often multi-specific, defined here as regulating several distinct processes⁸.

Here we focus on the multi-specific small GTPase Gsp1 (the *S. cerevisiae* homologue of human RAN) as a model system. Gsp1 (RAN) is a highly conserved molecular switch with one main GEF and one main GAP⁹ that regulates the nucleocytoplasmic transport of proteins¹⁰ and RNA¹¹, cell cycle progression¹² and RNA processing¹³. Crystal structures of Gsp1 (RAN) in complex with 16 different binding partners are known (Extended Data Fig. 1, Supplementary Fig. 1, Supplementary Table 1). We reasoned that by placing point mutations in Gsp1 interfaces with these partners, we would differentially perturb subsets of biological processes regulated by Gsp1. We then determined the functional consequences of these Gsp1 interface mutations on cellular processes in *S. cerevisiae* using quantitative genetic interaction mapping (Fig. 1a), measured changes to the physical interaction network using affinity

¹Department of Bioengineering and Therapeutic Sciences, University of California San Francisco, San Francisco, CA, USA. ²Quantitative Biosciences Institute (QBI), University of California San Francisco, San Francisco, CA, USA. ³European Molecular Biology Laboratory, European Bioinformatics Institute (EMBL-EBI), Cambridge, UK. ⁴The UC Berkeley–UCSF Graduate Program in Bioengineering, University of California San Francisco, San Francisco, CA, USA. ⁵Department of Cellular and Molecular Pharmacology, University of California San Francisco, San Francisco, CA, USA. ⁶The J. David Gladstone Institutes, San Francisco, CA, USA. ⁷Graduate Program in Bioinformatics, University of California San Francisco, San Francisco, California, USA. ⁸Program in Molecular Medicine, University of Massachusetts Medical School, Worcester, MA, USA. ⁹Department of Biochemistry and Molecular Pharmacology, University of Massachusetts Medical School, Worcester, MA, USA. ¹⁰Department of Pharmaceutical Chemistry, University of California San Francisco, San Francisco, CA, USA. ¹¹Chan Zuckerberg Biohub, San Francisco, CA, USA.

¹²These authors contributed equally: Tina Perica, Christopher J. P. Mathy. [✉]e-mail: nevan.krogan@ucsf.edu; kortemme@cgl.ucsf.edu

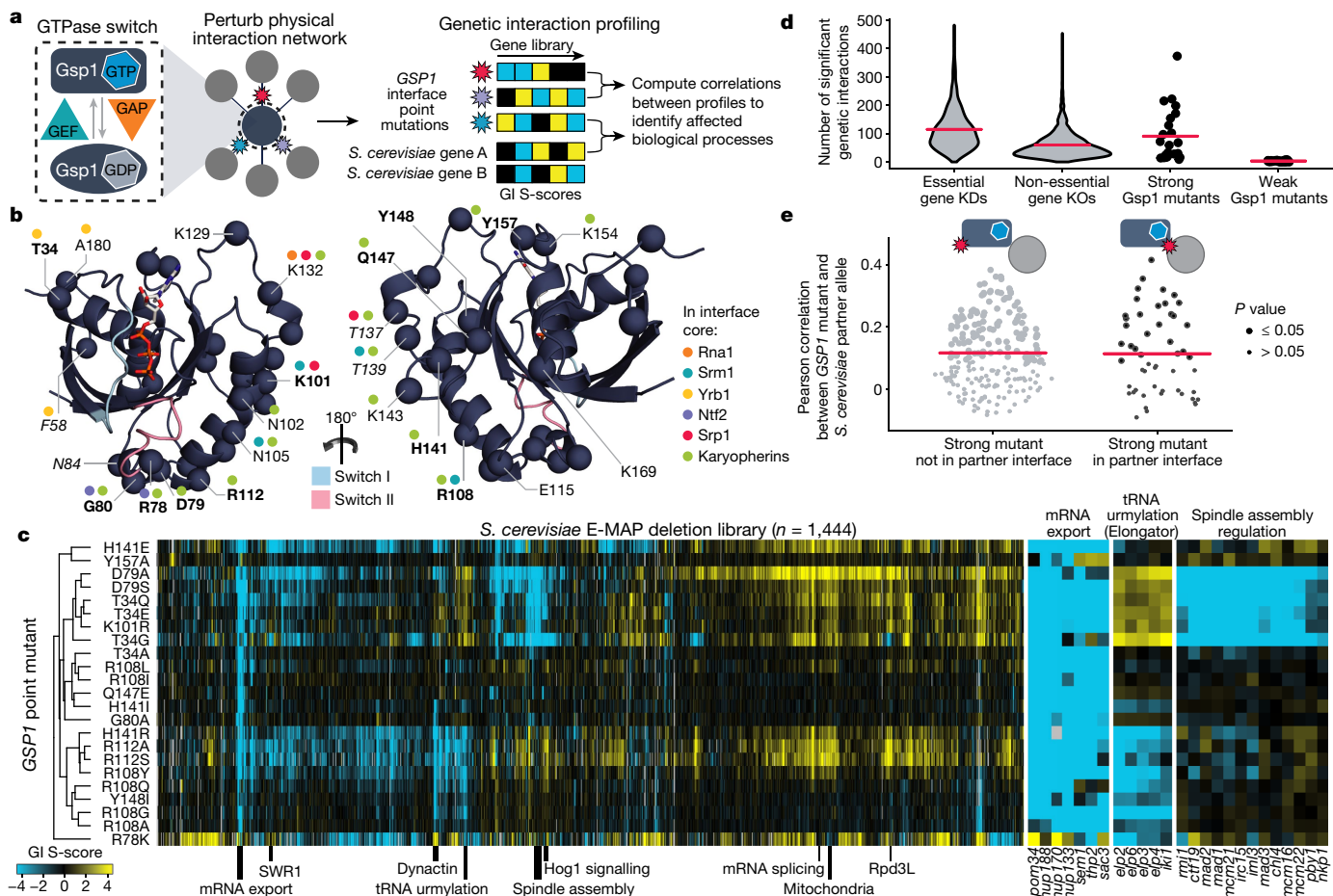


Fig. 1 | GI profiles of Gsp1 interface point mutants cluster by biological processes but not by targeted interfaces. **a**, Interface point mutations enable the probing of biological functions of the multi-specific GTPase switch Gsp1. **b**, Mutated residue positions shown as C α atom spheres on the structure of GTP-bound Gsp1. Bold font indicates the positions of mutations with strong GI profiles; italic font indicates the positions not conserved in the sequence between *S. cerevisiae* and human. Coloured dots, interaction partners for which the residue is in the interface core; blue and pink: switch I and switch II regions, respectively. **c**, GI profiles of 23 *GSP1* mutants with nine or more

significant GIs, hierarchically clustered by Pearson correlation. A negative S-score (blue) indicates synthetic sick or synthetic lethal GIs; a positive S-score (yellow) indicates suppressive or epistatic GIs. **d**, Distributions of significant GIs of *GSP1* point mutants compared to GIs of mutant alleles of essential and non-essential genes. **e**, Distributions of Pearson correlations between the GI profiles of Gsp1 interaction partners and *GSP1* mutants if mutation is (right, black) or is not (left, grey) in the interface with that partner. Point size corresponds to the false discovery rate (FDR)-adjusted one-sided (positive) *P* value of the Pearson correlation. Pink bars (**d**, **e**), mean.

purification mass spectrometry (AP-MS) and quantified molecular effects on the Gsp1 switch using biophysical studies in vitro.

Genetic interactions of Gsp1 mutants

We designed 55 genetically integrated point mutant alleles of *S. cerevisiae* *GSP1* to target each of its 16 known interactions (Fig. 1b, Extended Data Fig. 1, Supplementary Tables 2, 3), avoiding mutations in the Gsp1 nucleotide-binding site and the switch I and II regions. We confirmed by western blot that the mutant Gsp1 protein levels were close to the endogenous wild-type levels (Extended Data Fig. 2).

To determine the cellular effects of the *GSP1* interface mutations, we performed a genetic interaction (GI) screen in *S. cerevisiae* using the epistatic mini-array profile (E-MAP) approach^{5,7}. We measured the growth of each *GSP1* point mutant in the context of an array of 1,444 single-gene knockouts, resulting in a quantitative functional profile of up to 1,444 GI values for each *GSP1* point mutant (Supplementary Data 1). The 55 *GSP1* point mutants fell into two clusters: 23 ‘strong’ mutants with rich GI profiles containing 9–373 significant interactions (Fig. 1c); and 32 ‘weak’ mutants with 0–8 significant interactions (Extended Data Fig. 3, Methods, Supplementary Fig. 2). The strong mutants covered 11 Gsp1

sequence positions and all 16 structurally characterized Gsp1 protein interaction interfaces (Extended Data Fig. 4a). Twelve of the *GSP1* interface point mutants had a greater number of significant GIs than an average deletion of a non-essential *S. cerevisiae* gene, and six *GSP1* point mutants had more GIs than an average temperature-sensitive mutant of an essential gene in a published *S. cerevisiae* GI map¹⁴ (Fig. 1d). Hierarchical clustering of *S. cerevisiae* genes on the basis of their GIs with the *GSP1* interface mutations grouped genes by their cellular functions, including mRNA transport, tRNA modification and spindle assembly regulation (Fig. 1c, Extended Data Fig. 4b). Together, the GI analysis reveals extensive functional consequences of *GSP1* interface point mutations—similar in magnitude to effects that are typically observed for deleting entire genes—and helps to uncover many of the biological functions of *GSP1*.

In contrast to their clustering of biological processes, the GI profiles of the *GSP1* point mutants did not group on the basis of their location in the Gsp1 partner interfaces. For example, strains with *GSP1* mutations at residues T34 (T34E/Q) and D79 (D79S/A) have similar GI profiles (Fig. 1c), but these mutations are in different interfaces (Extended Data Fig. 4a) on opposite sides of the Gsp1 structure (Fig. 1b). This observation was contrary to our initial expectation that Gsp1 achieves its

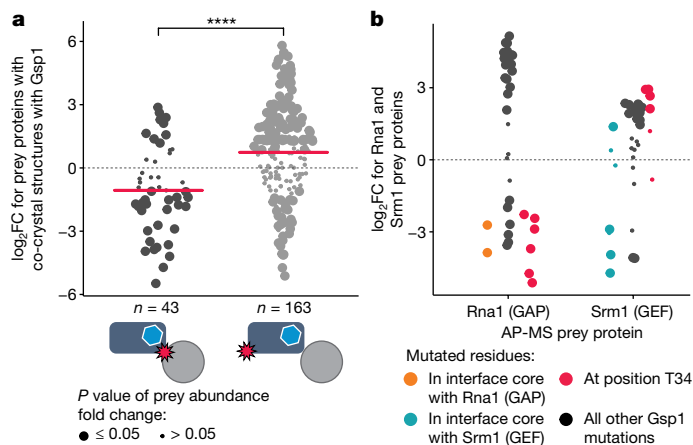


Fig. 2 | Gsp1 interface point mutations rewire the physical interaction network of Gsp1, including interactions with the switch regulators GEF (Srm1) and GAP (Rna1). Shown is the \log_2 -transformed fold change (' $\log_2\text{FC}$ ' in the figure) between the abundance of partner proteins pulled down with a Gsp1 mutant versus those pulled down with wild-type Gsp1. **a**, Change in abundance of partner proteins with crystal structures in complex with Gsp1 (Rna1, Srm1, Yrb1, Kap95, Pse1, Srp1) in which the mutation is (left) or is not (right) in the interface core with the partner. n refers to the number of partner abundance changes in each category. The mean \log_2 -transformed fold change values (pink bars) are -1 and 0.73 , respectively (t -test P value = 1.6×10^{-5}). Point size corresponds to the P value of abundance fold change. **b**, Change in abundance of pulled-down Rna1 and Srm1. Point size as in **a**; points coloured by interface location.

functional specificity by interacting with different partners. To analyse this finding further, we compared the *GSP1* mutant GI profiles to profiles from 3,370 *S. cerevisiae* alleles¹⁴ using Pearson correlations. Significant positive correlations of GI profiles indicate functional relationships⁵ (Supplementary Data 2, Supplementary Table 4, Extended Data Fig. 4c). Notably, GI profiles of *GSP1* mutants and of Gsp1 physical interaction partners were on average no more similar to each other in instances in which the Gsp1 mutation was located in the partner interface than in instances in which the mutation was not (Fig. 1e, Extended Data Fig. 4d). This result suggests that the rich functional profiles of *GSP1* mutants cannot simply be explained by considering only the partner interaction targeted by the interface point mutation.

Physical interactions of Gsp1 mutants

To investigate further why the GI profiles of *GSP1* mutations did not group based on targeted physical interactions of Gsp1, we sought to determine how interface point mutations affected the physical protein interaction network of Gsp1. We tagged wild-type Gsp1 and 28 mutants covering all interface residues shown in Extended Data Fig. 4a with an amino- or carboxy-terminal 3×Flag tag and quantified the abundance of 316 high-confidence 'prey' partner proteins in complex with Gsp1 by AP-MS (Fig. 2, Extended Data Fig. 5, Supplementary Data 3). We refer to the prey partner protein abundance in the pulled-down Gsp1 complexes simply as 'abundance' below. Six of the 16 Gsp1 binding partners for which we had structural information were robustly observable in the AP-MS data for both wild-type Gsp1 and Gsp1 mutants: the two core regulators Rna1 (GAP) and Srm1 (GEF), as well as four effectors Yrb1, Kap95, Pse1 and Srp1. As expected, the abundance of the prey partner was decreased on average (although not always) when the Gsp1 mutation was in the interface core with the prey partner (Fig. 2a, left distribution). However, instead of expected minimal effects, we also found notable changes in prey abundance in cases in which the mutation was not directly in the interface (Fig. 2a, right distribution). A wide spread of abundance changes was apparent for the two main

GTPase regulators, GAP (Rna1) and GEF (Srm1), even for mutations at positions that are outside either of the interfaces such as T34 (Fig. 2b, Extended Data Fig. 6, Supplementary Table 5). In summary, the AP-MS experiments show that the point mutations, in addition to affecting the targeted interactions, also introduce extensive changes to the physical interaction network of Gsp1 that cannot simply be explained by the interface location of the mutations.

Effect of mutants on Gsp1 switch kinetics

The AP-MS experiments showed that most Gsp1 interface mutations significantly altered physical interactions with the two principal GTPase regulators, GAP and GEF. This observation prompted us to ask whether the mutations, rather than acting indirectly in the cellular context (that is, by altering the competition between physical interaction partners in the cell), affected the molecular function of the switch directly. To assess the molecular effects of mutations on switch function, we recombinantly expressed and purified wild-type Gsp1 and 24 Gsp1 mutants and measured their effects on GAP-mediated GTP hydrolysis and GEF-mediated nucleotide exchange in vitro (Fig. 3a, b, Extended Data Fig. 7, Supplementary Figs. 3, 4, Supplementary Tables 6, 7). Of the 24 Gsp1 point mutants, 17 (of which all except K132H had strong GI profiles) showed a change of 3-fold to more than 200-fold in catalytic efficiency (k_{cat}/K_m) on either or both of the GAP- or GEF-mediated reactions (Extended Data Fig. 7e). These results show that Gsp1 interface mutations can modulate the GTPase cycle by affecting GTP hydrolysis and nucleotide exchange catalysed by the GAP and GEF. Moreover, as 9 out of the 17 mutations with larger than 3-fold effects are located outside of the interface cores with either the GAP (Fig. 3a) or the GEF (Fig. 3b) as well as outside the known switch regions, our data suggest considerable, previously unappreciated, allostericity in the GTPase switch.

Allosteric effects of mutations

To probe the mechanism of these allosteric effects, we examined the effect of Gsp1 point mutations on the conformational distribution in the active site of GTP-bound Gsp1 using 1D ^{31}P nuclear magnetic resonance (NMR) spectroscopy. Previous ^{31}P NMR data on human RAN¹⁵ showed two distinct peaks for the γ -phosphate of bound GTP arising from differences in the local chemical environment of the γ -phosphate in each of two distinct conformations (termed $\gamma 1$ and $\gamma 2$). Our ^{31}P NMR spectra of *S. cerevisiae* wild-type Gsp1–GTP showed two distinct peaks for the γ -phosphate of bound GTP, with 87% of wild-type Gsp1–GTP in the $\gamma 2$ state conformation (Fig. 3c, Extended Data Fig. 8a). Of note, the relative populations of the $\gamma 1$ and $\gamma 2$ states were modulated by our Gsp1 interface mutations and ranged from close to 0% in the $\gamma 2$ state for T34E and T34Q, to close to 100% for H141R, Y157A and K132H (Fig. 3c).

Furthermore, we observed a linear relationship between the effect of the mutation on the equilibrium between the $\gamma 1$ and $\gamma 2$ conformations (plotted as the natural log-transformed ratio of the equilibrium constant) and the natural log-transformed ratio of the relative catalytic efficiencies of GAP-mediated GTP hydrolysis (Fig. 3d) and intrinsic GTP hydrolysis (Extended Data Fig. 8b, c, Supplementary Table 8). This relationship suggests that the $\gamma 2$ state represents the active site conformation of Gsp1–GTP competent for GTP hydrolysis. Exceptions to the linear relationship are K132H, which is in the core of the GAP interface and hence expected to directly affect the interaction with the GAP; and D79S and R78K, which are adjacent to the GTPase switch II region and could lead to different perturbations of the nucleotide-binding site.

The mutated residues that tune the population of the $\gamma 2$ state (positions T34, H141, Q147 and Y157) are all distal, affecting the chemical environment of the Gsp1-bound GTP γ -phosphate from at least 18 Å away (Extended Data Fig. 8d, e). Together, our in vitro data support an allosteric mechanism in which distal mutations at different surface interaction sites of Gsp1 modulate the GTPase switch by differentially

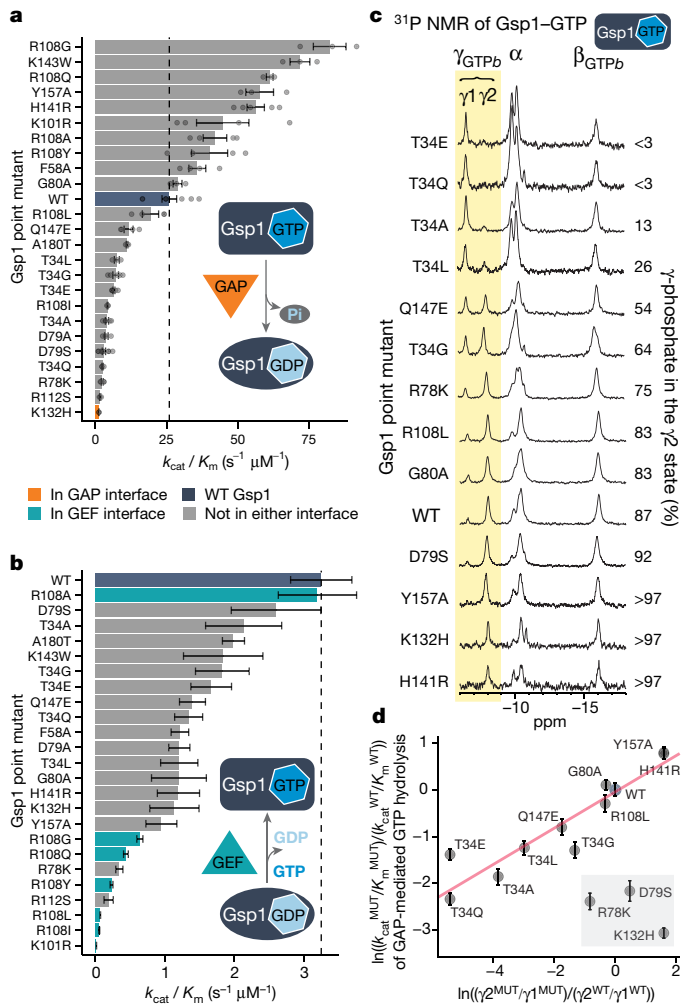


Fig. 3 | Point mutations in Gsp1 interfaces allosterically modulate GTPase cycle parameters by tuning active site conformational distributions.

a, b, Catalytic efficiency (k_{cat}/K_m) of GAP-mediated GTP hydrolysis (a) or GEF-mediated nucleotide exchange (b) of Gsp1 mutants. Dotted lines indicate the wild-type (WT) efficiency. In a, points represent k_{cat}/K_m from an individual experiment fit to an integrated Michaelis–Menten equation. Error bars, s.e.m. from $n \geq 3$ replicates. In b, error bars are the s.e.m. of the Michaelis–Menten fit to data from $n \geq 17$ measurements at different substrate concentrations. **c**, ^{31}P NMR of GTP-bound Gsp1 point mutants. NMR peak heights are normalized to the β -peak of bound GTP (β_{GTPb}). The two peaks of the γ -phosphate of bound GTP are highlighted in yellow. **d**, Natural log (ln)-transformed ratios (mutant to wild-type; MUT/WT) of the exchange equilibrium constants (K_{ex} = population in $\gamma 2$ /population in $\gamma 1$ (assuming a detection limit of 3% for the γ -peak estimation by ^{31}P NMR)) plotted against the natural log-transformed ratios (MUT/WT) of the relative catalytic efficiency (k_{cat}/K_m) of GAP-mediated GTP hydrolysis. Error bars, s.e.m. from $n \geq 3$ replicates. Pink line, least-squares linear fit, excluding K132H, R78K and D79S (grey box).

affecting GEF-catalysed nucleotide exchange and GAP-catalysed GTP hydrolysis. Moreover, comparison between the in vitro kinetic and our AP-MS data showed that the direction of the GTPase cycle perturbation is a good predictor of altered physical interactions with the two main cycle regulators (Extended Data Fig. 9), even in the context of other potentially competing partner proteins.

Encoding of Gsp1 multi-specificity

Finally, we asked whether the allosteric effects of the mutations on the GTPase cycle kinetics explained the functional effects observed in the

cellular GI profiles. This analysis also provided insights into the ability of Gsp1 to distinctly regulate different biological processes (functional multi-specificity). We clustered the GI profiles of the *GSP1* mutants on the basis of correlation with the GI profiles of 3,358 *S. cerevisiae* alleles;¹⁴ 276 alleles had significant correlations with *GSP1* mutants (Fig. 4a). We then compared the clustering of these GI profile correlations with the biophysical effects of the Gsp1 mutations. Notably, the *GSP1* mutant GI profile clustering mirrored an approximate ordering by the in vitro mutant effects on the GTPase cycle: relative GAP efficiency systematically increased with increasing column number and relative GEF efficiency decreased (Fig. 4a). (The clear outlier, K101R, could be explained by acetylation of this residue¹⁶. The K101R mutation could affect a critical mechanism by which the cell reduces GEF activity¹⁷, phenocopying mutants with reduced GTP hydrolysis activity.) Overall, genes in Fig. 4a fall into one of three categories: (i) genes in cluster 1, but also cluster 2, that correlate with mutants primarily perturbed in GTP hydrolysis (Fig. 4a, orange bars); (ii) genes in cluster 7 that correlate with mutants primarily perturbed in nucleotide exchange (teal bars); and (iii) genes that correlate strongly with all or most of the *GSP1* point mutants (cluster 5, but also clusters 3, 4, and 6).

Genes with shared biological functions (gene sets; Supplementary Data 4) all predominantly fall into one of the three categories defined above. For example, genes involved in spindle assembly regulation have significant GI profile correlations primarily with *GSP1* mutant group I (Fig. 4b, red points), genes involved in tRNA modification correlate primarily with *GSP1* mutant group III (blue points) and genes important for nucleocytoplasmic transport correlate with *GSP1* mutants from all three groups (green points). The three groups of Gsp1 mutants show distinct kinetic characteristics: group I has decreased efficiency of GTP hydrolysis; group III has decreased efficiency of nucleotide exchange; and group II shows intermediate behaviour (Fig. 4c). Therefore, our analysis suggests that distinct cellular processes regulated by Gsp1, such as spindle assembly regulation, tRNA modification and nuclear transport (Fig. 4b, d), as well as 5' mRNA capping, transcriptional regulation, cytoplasm-to-vacuole targeting and actin, tubulin and cell polarity (Extended Data Fig. 10), are differentially sensitive to perturbations of GTPase cycle kinetics. Together, our findings lead to a model in which Gsp1 acts by three different modes defined by the sensitivity of different biological processes to perturbations of different characteristics of the Gsp1 GTPase cycle, that is, the ability to (i) cycle; (ii) turn off by hydrolysing to Gsp1-GDP; and (iii) turn on by producing Gsp1-GTP (Fig. 4d). Although other effects such as changes in interaction affinities or expression levels undoubtedly also have a role in modulating the functional effects of our Gsp1 mutations, our model explains to a considerable extent how a single molecular switch motif can differentially control subsets of biological processes by using one of the three functional modes.

Discussion

The discovery of several new allosteric sites (positions 34, 141, 147, and 157) in Gsp1 has implications for GTPase regulation. Our finding that mutations in Gsp1 interfaces allosterically modulate the switch cycle identifies thermodynamic coupling between distal interfaces and the active site; partner binding or post-translational modifications at these distal sites could also regulate the switch.

Our observation of widespread functional effects of point mutations inducing relatively small perturbations in the GTPase switch kinetics is reminiscent of the zero-order ultrasensitivity that is achievable in biological motifs with opposing regulators². Although switch-like ultrasensitivity is typically described for systems that are controlled by covalent modifications (such as phosphorylation), our results—as well as the observations that cellular levels of small GTPase regulators require tight control^{18,19}—corroborate a model of ultrasensitivity for GTPase conformational switches²⁰.

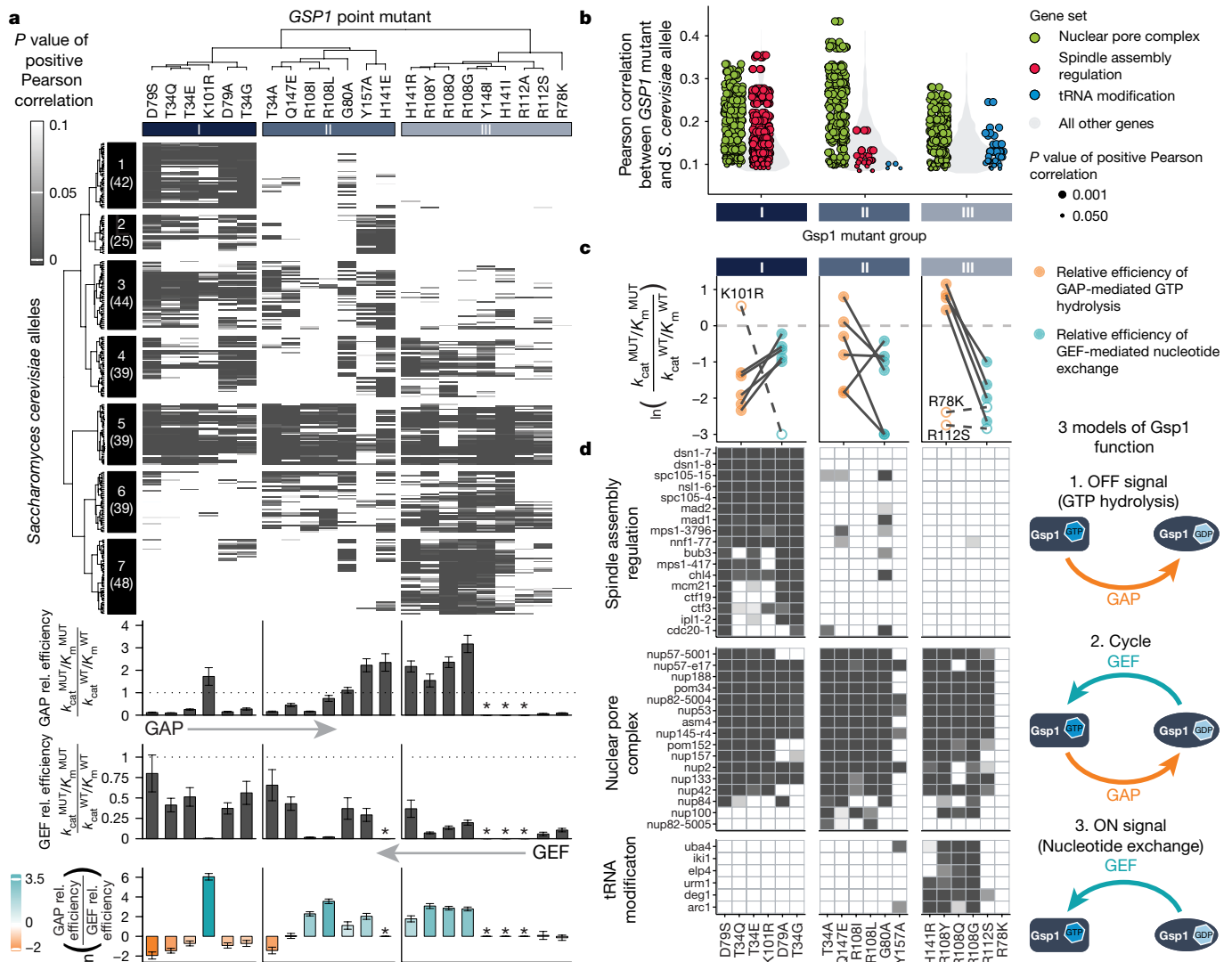


Fig. 4 | Cellular effects of interface mutations group by their effect on GTPase cycle kinetics. **a**, Clustering of 276 *S. cerevisiae* alleles and 22 strong *GSP1* point mutants by the P value of Pearson correlations of their GI profiles compared to the relative efficiencies of GAP-mediated GTP hydrolysis and GEF-mediated nucleotide exchange (asterisks, not measured). Grey scale: FDR-adjusted one-sided (positive) P value of the Pearson correlations. Numbers in parentheses indicate the number of genes in the cluster. **b**, Distributions of Pearson correlations, separated by *GSP1* point mutant groups from column hierarchical clustering in a. Green, red or blue points are individual correlations with *S. cerevisiae* genes in three gene sets; grey violin

plots show distributions of correlations with all other genes; point size corresponds to the FDR-adjusted one-sided (positive) P value of the Pearson correlation. Only significant correlations (P value < 0.05) are included. **c**, Kinetic characteristics of Gsp1 mutant groups I to III. Outliers are shown as empty circles and dashed lines. The log ratio of relative catalytic efficiencies is capped at -3. **d**, Heatmaps of the FDR-adjusted one-sided (positive) P value of the Pearson correlation for the three representative gene sets. *S. cerevisiae* genes for each gene set are clustered by P value. The GTPase cycle schemes on the right represent three modes of Gsp1 function. In c, d, only Gsp1 mutants with kinetics data are shown, grouped as in a.

Given the prevalence of biological two-state switch motifs with opposing regulators (kinase–phosphatase, acetylase–deacetylase), we envision that our approach to engineer defined molecular perturbations and characterize them with systems-level functional genetics integrated with molecular biophysics will be informative for other studies of cellular regulation. The approach could be extended to mammalian systems using CRISPR-based approaches to yield mechanistic insights into the consequences of disease mutations targeting central molecular switches.

Online content

Any methods, additional references, Nature Research reporting summaries, source data, extended data, supplementary information, acknowledgements, peer review information; details of author contributions

and competing interests; and statements of data and code availability are available at <https://doi.org/10.1038/s41586-021-03982-6>.

1. Ferrell, J. E. & Ha, S. H. Ultrasensitivity part I: Michaelian responses and zero-order ultrasensitivity. *Trends Biochem. Sci.* **39**, 496–503 (2014).
2. Goldbeter, A. & Koshland, D. E. An amplified sensitivity arising from covalent modification in biological systems. *Proc. Natl. Acad. Sci. USA* **78**, 6840–6844 (1981).
3. Eisenberg, D., Marcotte, E. M., Xenarios, I. & Yeates, T. O. Protein function in the post-genomic era. *Nature* **405**, 823–826 (2000).
4. Rush, M. G., Drivas, G. & D'Eustachio, P. The small nuclear GTPase Ran: how much does it run? *BioEssays* **18**, 103–112 (1996).
5. Collins, S. R., Schuldiner, M., Krogan, N. J. & Weissman, J. S. A strategy for extracting and analyzing large-scale quantitative epistatic interaction data. *Genome Biol.* **7**, R63 (2006).
6. Braberg, H. et al. Genetic interaction mapping informs integrative structure determination of protein complexes. *Science* **370**, eaaz4910 (2020).
7. Braberg, H. et al. From structure to systems: high-resolution, quantitative genetic analysis of RNA polymerase II. *Cell* **154**, 775–788 (2013).
8. Dasso, M. The Ran GTPase: theme and variations. *Curr. Biol.* **12**, R502–R508 (2002).

9. Bischoff, F. R. & Ponstingl, H. in *The Small GTPase Ran* Vol. 1 (eds Rush, M. & D'Eustachio, P.) 163–176 (Springer, 2001); https://doi.org/10.1007/978-1-4615-1501-2_9
10. Moore, M. S. & Blobel, G. The GTP-binding protein Ran/TC4 is required for protein import into the nucleus. *Nature* **365**, 661–663 (1993).
11. Köhler, A. & Hurt, E. Exporting RNA from the nucleus to the cytoplasm. *Nat. Rev. Mol. Cell Biol.* **8**, 761–773 (2007).
12. Arnaoutov, A. & Dasso, M. The Ran GTPase regulates kinetochore function. *Dev. Cell* **5**, 99–111 (2003).
13. Ren, M. et al. Separate domains of the Ran GTPase interact with different factors to regulate nuclear protein import and RNA processing. *Mol. Cell. Biol.* **15**, 2117–2124 (1995).
14. Costanzo, M. et al. A global genetic interaction network maps a wiring diagram of cellular function. *Science* **353**, aaf1420 (2016).
15. Geyer, M. et al. Conformational states of the nuclear GTP-binding protein Ran and its complexes with the exchange factor RCC1 and the effector protein RanBP1. *Biochemistry* **38**, 11250–11260 (1999).
16. Henriksen, P. et al. Proteome-wide analysis of lysine acetylation suggests its broad regulatory scope in *Saccharomyces cerevisiae*. *Mol. Cell. Proteomics* **11**, 1510–1522 (2012).
17. de Boor, S. et al. Small GTP-binding protein Ran is regulated by posttranslational lysine acetylation. *Proc. Natl. Acad. Sci. USA* **112**, E3679–E3688 (2015).
18. Besray Unal, E. et al. Systems level expression correlation of Ras GTPase regulators. *Cell Commun. Signal.* **16**, 46 (2018).
19. Görlich, D., Seewald, M. J. & Ribbeck, K. Characterization of Ran-driven cargo transport and the RanGTPase system by kinetic measurements and computer simulation. *EMBO J.* **22**, 1088–1100 (2003).
20. Barr, F. A. Review series: Rab GTPases and membrane identity: causal or inconsequential? *J. Cell Biol.* **202**, 191–199 (2013).

Publisher's note Springer Nature remains neutral with regard to jurisdictional claims in published maps and institutional affiliations.

© The Author(s), under exclusive licence to Springer Nature Limited 2021

Methods

Additional Methods

Detailed Methods are provided in the Supplementary Methods and additional analysis can be found in the Supplementary Discussion.

Point mutations in the genomic *Gsp1* sequence

We identified all residues in *Gsp1* that comprised the interfaces with *Gsp1* binding partners for which co-complex crystal structures with *Gsp1* were available (Supplementary Fig. 1, Extended Data Fig. 1, Supplementary Table 1). Residues comprising the interface ‘core’, the surface exposed ‘rim’ around the core, and more buried ‘support’ residues were defined on the basis of per-residue relative solvent accessible surface area (rASA), as previously described²¹. Avoiding positions in the canonical P-loop or in the switch I or II regions²², we mutated residues that are located in interface cores (Supplementary Table 2, Extended Data Fig. 1g) into amino acid residues with a range of properties (differing in size, charge and polarity) and attempted to make stable and viable *S. cerevisiae* strains carrying a genomic *GSP1* point mutation (Supplementary Fig. 5). The list of attempted mutants is provided in Supplementary Table 3.

Saccharomyces cerevisiae genetics and GI mapping

E-MAP of *Gsp1* point mutants. GIs of all viable *GSP1* point mutant (PM-*GSP1*-clonNAT) strains were identified by E-MAP screens^{23,24} using a previously constructed array library of 1,536 KAN-marked (kanamycin) mutant strains assembled from the *S. cerevisiae* deletion collection²⁵ and the DAmP (decreased abundance by mRNA perturbation) strain collection²⁶, covering genes involved in a wide variety of cellular processes⁷. The E-MAP screen was conducted as previously described²³. GI scores represent the average of 3–5 independent replicate screens. Reproducibility was assessed as previously described⁵ by comparing individual scores to the average score for each mutant–gene pair, with the two values showing strong correlation across the dataset (Pearson correlation coefficient = 0.83, Supplementary Fig. 6).

Hierarchical clustering of E-MAP GI data. All E-MAP library DAmP strains as well as library strains showing poor reproducibility were discarded, leaving 1,444 out of the original 1,536 library genes. Averaged S-scores of GIs between wild-type and point mutant *GSP1* and the 1,444 *S. cerevisiae* genes are provided in Supplementary Data 1. Hierarchical clustering on the GI profiles was performed using the average linkage method and the pairwise Pearson correlation coefficient as a distance metric. To identify clusters of functionally related library genes, the hierarchical clustering tree was cut to produce 1,200 clusters, which resulted in 43 clusters with 3 or more members. Biological function descriptions for genes in these clusters were extracted from the *Saccharomyces* Genome Database (SGD)²⁷. Clusters of genes representing common functions (complexes, pathways or biological functions) were selected by manual inspection and represented in Fig. 1c, Extended Data Fig. 4b.

GI profile correlation measurements. Of the 1,444 library genes in the *GSP1* point mutant GI profile map, 1,129 were present in the synthetic genetic array (SGA) dataset¹⁴. Pairwise Pearson correlation coefficients were computed between all *GSP1* point mutants and SGA gene profiles, and all profiles were trimmed to include only GI measurements with the 1,129 shared library genes. Owing to the relative sparsity of GI profiles, pairwise comparisons are dominated by high numbers of non-significant interactions. Accordingly, we did not consider correlations with *GSP1* point mutants or SGA gene profiles that did not have significant GIs (absolute scaled S-score greater than 3; see Supplementary Methods) with at least 10 of the 1,129 library genes. This requirement removed all weak *GSP1* point mutants and one strong mutant (R108A) from the correlation analysis (as they had at most 9 GIs

with an absolute score greater than 3), leaving 22 strong mutants and 3,370 *S. cerevisiae* SGA alleles to be included in the correlation analysis. All Pearson correlations and their *P* values between *GSP1* mutants and *S. cerevisiae* genes, including all correlations that did not pass our significance filtering procedures, are provided in Supplementary Data 2. The subset of Pearson correlations between *GSP1* point mutants and *Gsp1* partners with available co-complex X-ray crystal structures, used to make the point plots in Fig. 1e, Extended Data Fig. 4c, d, are also available in Supplementary Table 4.

The statistical significance of correlations was computed using both two-sided and one-sided (positive) *t*-tests adjusted for multiple hypothesis testing using both the Bonferroni method and the FDR method, which controls the false discovery rate²⁸. All *P* values reported in the text and figures are one-sided (positive) and corrected by the FDR method, unless otherwise stated. The FDR method of *P* value correction has been shown to account for the positive dependency between test statistics²⁹, such as those arising from the underlying functional similarities between *S. cerevisiae* alleles.

Significance testing was used to filter out *S. cerevisiae* gene SGA profiles that did not show a significant correlation (one-sided positive, Bonferroni-adjusted) with the GI profiles of at least two *GSP1* point mutants. In total, 276 *S. cerevisiae* alleles from the SGA had a significant GI profile correlation (one-sided positive, Bonferroni-adjusted) with at least two *GSP1* point mutants and were therefore included in the correlation analysis shown in Fig. 4a. We required alleles to correlate with at least two mutants because the goal of this analysis was to group mutants by similarity, and an allele that only significantly correlated with one mutant is uninformative for this task. After this filtering step, the one-sided *P* values were used to populate a matrix of 22 mutants versus 276 alleles, and hierarchical clustering was performed using Ward’s method. We used Ward’s method rather than the average linkage criterion as we found that the latter resulted in a wide variety of group sizes owing to a few sparsely populated outliers. Using Ward’s method resulted in rounder clusters, allowing us to identify meaningful functional groups of mutants and alleles. Pearson correlation between correlation vectors was used as a distance metric for the mutant (row) clustering, and Euclidean distance was selected for the gene (column) clustering, owing to the column vectors being relatively short (22 mutants per column versus 276 alleles per row) and thus sensitive to outliers when clustered using Pearson correlations as the distance metric (for additional analysis of E-MAP statistics and clustering, see Supplementary Discussion).

For the gene set analysis, we decreased the stringency of inclusion of *S. cerevisiae* SGA genes to include all alleles with a significant GI profile correlation (one-sided positive, Bonferroni-adjusted) with one or more *GSP1* mutants, which added another 201 alleles, resulting in 477 alleles. We made the gene sets larger to increase our confidence in connecting the patterns of correlations between *S. cerevisiae* genes and *GSP1* mutants, and GTPase cycle parameters represented in Fig. 4b, d. Indeed, although *S. cerevisiae* genes that only correlate significantly with one mutant are not informative for grouping mutants, they are informative for annotating the functional effects of individual mutants. Manually curated gene sets of *S. cerevisiae* genes with significant correlations with *GSP1* mutants are provided in Supplementary Data 4.

Physical interaction mapping using AP-MS

***S. cerevisiae* cell lysate preparation.** *S. cerevisiae* strains for AP-MS were grown in YAPD medium (120 mg adenine hemisulfate salt (A9126, Sigma), 10 g Bacto yeast extract (BD 212720), 20 g Bacto peptone (BD 211820) and 20 g dextrose (D-glucose D16-3, Fisher Chemicals) per 1 l of medium). Each strain was grown at 30 °C for 12 to 24 h to an optical density at 600 nm (OD_{600}) of 1–1.5. The cells were collected by centrifugation at 3,000*g* for 3 min and the pellet was washed in 50 ml of ice-cold ddH₂O, followed by a wash in 50 ml of 2× lysis buffer (200 mM HEPES pH 7.5, 200 mM KCl, 2 mM MgCl₂, 30 μM GTP (guanosine 5'-triphosphate

sodium salt hydrate, G8877, Sigma-Aldrich), 1 mM dithiothreitol (Promega V3151), 0.1% IGEPAL CA-630 (I8896, Sigma-Aldrich), and 10% glycerol). Each pellet of approximately 500 µl was then resuspended in 500 µl of 2× lysis buffer supplemented with protease inhibitors without EDTA (cOmplete, Mini, EDTA-free Protease Inhibitor Cocktail, 11836170001, Roche) and dripped through a syringe into liquid nitrogen. The frozen *S. cerevisiae* cell pellets were lysed in liquid nitrogen with a SPEX SamplePrep 6870 Freezer/Mill.

Flag immunoprecipitations were performed as previously described^{30,31}.

Liquid chromatography with tandem mass spectrometry analysis.

To prepare samples for liquid chromatography with tandem mass spectrometry (LC-MS/MS) analysis, immunoprecipitated protein (10 µl) was denatured and reduced in 2 M urea, 10 mM NH₄HCO₃, and 2 mM dithiothreitol for 30 min at 60 °C with constant shaking, alkylated in the dark with 2 mM iodoacetamide for 45 min at room temperature and digested overnight at 37 °C with 80 ng trypsin (Promega). After digestion, peptides were acidified with formic acid and desalted using C18 ZipTips (Millipore) according to the manufacturer's specifications. Samples were resuspended in 4% formic acid, 2% acetonitrile solution, and separated by a 75-min reversed-phase gradient over a nanoflow C18 column (Dr. Maisch). Peptides were directly injected into a Q-Exactive Plus mass spectrometer (Thermo Fisher Scientific), with all MS1 and MS2 spectra collected in the orbitrap. Raw MS data were searched against the *S. cerevisiae* proteome (SGD sequences downloaded on 13 January 2015) using the default settings in MaxQuant (v.1.5.7.4), with a match-between-runs enabled^{32,33}. Peptides and proteins were filtered to 1% FDR in MaxQuant, and identified proteins were then subjected to protein–protein interaction scoring using SAINTexpress³⁴. Proteins were filtered to only those representing high confidence protein–protein interactions (Bayesian FDR from SAINT (SAINT BFDR) < 0.05). Protein abundance values for this filtered list were then subjected to equalized median normalization, and label-free quantification and statistical analysis were performed using MSstats³⁵, separately for data from amino- or carboxy-terminally tagged baits. The fold change in abundance of prey proteins for 3×Flag-tagged Gsp1 point mutants was always calculated compared to the wild-type Gsp1 with the corresponding tag. All AP-MS data are available from the PRIDE repository under the PXD016338 identifier. Fold change values between prey abundance between the mutant and wild-type Gsp1 and the corresponding FDR-adjusted *P* values are provided in Supplementary Data 3. The intersection of all prey proteins identified at least once with both the amino- or carboxy-terminal 3×Flag tag, and their interquartile ranges of log₂-transformed fold change values across all the Gsp1 mutants, are provided in Supplementary Table 5. The quality of data and reproducibility between replicates was assessed on the basis of correlations of protein abundance between replicates (Supplementary Figs. 7, 8).

Biochemical and biophysical assays

Protein purifications. All proteins were expressed from a pET-28 a (+) vector with an N-terminal 6×His tag in *Escherichia coli* strain BL21(DE3) in the presence of 50 mg l⁻¹ of kanamycin for 2xYT medium, and 100 mg l⁻¹ of kanamycin for autoinduction EZ medium. GEF (Srm1 from *S. cerevisiae*; Uniprot P21827) was purified as Srm1(Δ1–27) and GAP (Rna1 from *S. pombe*; Uniprot P41391) as a full-length protein (for use of *S. pombe* Rna1 see Supplementary Discussion). ScSrm1(Δ1–27) and SpRna1 were expressed in 2xYT medium (10 g NaCl, 10 g yeast extract (BD Bacto Yeast Extract 212720), 16 g tryptone (Fisher, BP1421) per 1 l of medium) overnight at 25 °C upon addition of 300 µmol l⁻¹ isopropyl-β-D-thiogalactoside (IPTG). Gsp1 variants were expressed by autoinduction for 60 h at 20 °C in autoinduction medium, as described before³⁶.

Cells were lysed in 50 mM Tris pH 7.5, 500 mM NaCl, 10 mM imidazole and 2 mM β-mercaptoethanol using a microfluidizer from Microfluidics. For Gsp1 purifications, the lysis buffer was also supplemented

with 10 mM MgCl₂. The His-tagged proteins were purified on Ni-NTA resin (Thermo Fisher Scientific, 88222) and washed into a buffer containing 50 mM Tris (pH 7.5) and 100 mM NaCl, with 5 mM MgCl₂ for Gsp1 proteins. The N-terminal His-tag was digested at room temperature overnight using up to 12 NIH units per ml of bovine thrombin (Sigma-Aldrich T4648-10KU). Proteins were then purified using size-exclusion chromatography (HiLoad 26/600 Superdex 200 pg column from GE Healthcare), and purity was confirmed to be at least 90% by SDS-PAGE. Samples were concentrated on 10-kDa spin filter columns (Amicon, UFC901024) into storage buffer (50 mM Tris pH 7.5, 150 mM NaCl, 1 mM dithiothreitol). Storage buffer for Gsp1 proteins was supplemented with 5 mM MgCl₂.

GTP loading of Gsp1. Gsp1 variants for GTPase assays as well as for ³¹P NMR spectroscopy were first loaded with GTP by incubation in the presence of 20-fold excess GTP (guanosine 5'-triphosphate, disodium salt, 371701, Calbiochem) in 50 mM Tris HCl pH 7.5, 100 mM NaCl, 5 mM MgCl₂. Exchange of GDP for GTP was initiated by the addition of 10 mM EDTA. Reactions were incubated for 3 h at 4 °C and stopped by the addition of 1 M MgCl₂ to a final concentration of 20 mM MgCl₂ to quench the EDTA. GTP-loaded protein was buffer-exchanged into either NMR buffer or the GTPase assay buffer using NAP-5 Sephadex G-25 DNA Grade columns (GE Healthcare, 17085301).

NMR spectroscopy. Gsp1 samples for ³¹P NMR spectroscopy were first loaded with GTP as described above, and buffer-exchanged into NMR buffer (D₂O with 50 mM Tris-HCl pH 7.4, 5 mM MgCl₂, 2 mM dithiothreitol). Final sample concentrations were between 250 µM and 2 mM, and 400 µl of samples were loaded into 5-mm Shigemi advanced microtubes matched to D₂O (BMS-005TB; Shigemi). ³¹P NMR experiments were performed on a Bruker Avance III 600 MHz NMR spectrometer with a 5-mm BBFO Z-gradient probe. Spectra were acquired and processed with the Bruker TopSpin software (v.4.0.3). Indirect chemical shift referencing for ³¹P to DSS (2 mM Sucrose, 0.5 mM DSS, 2 mM NaN₃ in 90% H₂O + 10% D₂O; water-suppression standard) was done using the IUPAC-IUB recommended ratios³⁷. Spectra were recorded at 25 °C using the pulse and acquire program zg (TopSpin 3.6.0), with an acquisition time of 280 ms, a recycle delay of 3.84 s and a 65° hard pulse. A total of 4,096 complex points were acquired over the course of 4,096 scans and a total acquisition time of 4.75 h. Spectra were zero-filled once and multiplied with an exponential window function (EM) with a line-broadening of 6 Hz (LB = 6) before Fourier transformation. Peaks were integrated using the auto-integrate function in TopSpin 4.0.7, and peak areas were referenced to the bound GTP-β peak of each spectrum. The peak at approximately -7 ppm is defined as γ1 and the peak at approximately -8 ppm is defined as γ2. The percentage of γ phosphate in γ2 is defined as a ratio of areas under the curve between the γ2 and the sum of the γ1 and γ2 peaks.

Kinetic measurements of GTP hydrolysis. Kinetic parameters of the GTP hydrolysis reaction were determined using a protocol similar to one previously described³⁸. Gsp1 samples for GTP hydrolysis kinetic assays were first loaded with GTP as described above. GTP hydrolysis was monitored by measuring fluorescence of the *E. coli* phosphate-binding protein labelled with 7-diethylamino-3-[*N*-(2-maleimidooethyl)carbamoyl]coumarin (MDCC) (phosphate sensor; PV4406, Thermo Fisher Scientific) upon binding of the free phosphate GTP hydrolysis product (excitation at 425 nm, emission at 457 nm). All experiments were performed in GTPase assay buffer (40 mM HEPES pH 7.5, 100 mM NaCl, 4 mM MgCl₂, 1 mM dithiothreitol) at 30 °C in a 100-µl reaction volume on a Synergy H1 plate reader from BioTek, using Corning 3881 96-well half-area clear-bottom non-binding surface plates. For each individual GAP-mediated GTP hydrolysis experiment, a control experiment with the same concentration of GTP-loaded Gsp1 and the same concentration of sensor, but without added GAP, was run in parallel. The first 100 s of these data were used to determine the baseline fluorescence,

Article

and the rest of the data were linearly fitted to estimate the intrinsic GTP hydrolysis rate (Supplementary Table 1).

Estimating the k_{cat} and K_m parameters of GAP-mediated hydrolysis. We used an analytical solution of the integrated Michaelis–Menten equation based on the Lambert ω function, as described before³⁹, to estimate the k_{cat} and K_m of GAP-mediated GTP hydrolysis. The curves were fit with the custom-made software DELA⁴⁰. Examples of full reaction progress curves and their integrated Michaelis–Menten fits are shown in Supplementary Fig. 3.

For most mutants a concentration of 1 nM GAP (*SpRna1*, *Rna1* from *S. pombe*) was used. To run the time courses to completion, for mutants with low k_{cat}/K_m enzyme concentrations of 2–5 nM were used. Initially we collected time-course data for all *Gsp1* variants at an approximately 8 μM concentration of loaded *Gsp1*–GTP with 1 nM GAP and 20 μM phosphate sensor. If the estimated K_m was higher than 1 μM, we repeated the time-course kinetic experiments with a higher concentration of *Gsp1*–GTP of approximately 10-fold above the K_m .

The Michaelis–Menten k_{cat} and K_m parameters and their standard deviations were calculated from at least three technical replicates from two or more independently GTP-loaded *Gsp1* samples (Supplementary Table 6). For more details on the kinetic analysis, see Supplementary Discussion, Supplementary Methods.

Kinetic measurements of Srm1-mediated nucleotide exchange. Kinetic parameters of GEF-mediated nucleotide exchange were determined using a fluorescence resonance energy transfer (FRET)-based protocol⁴¹. Nucleotide exchange from GDP to mant-GTP (2’-(or-3’)-O-(N-methylanthraniloyl) guanosine 5’-triphosphate, NU-206L, Jena Biosciences) was monitored by measuring a decrease in intrinsic *Gsp1* tryptophan fluorescence (295 nm excitation, 335 nm detection) due to FRET upon binding of the mant group. Each time course was measured in GEF assay buffer (40 mM HEPES pH 7.5, 100 mM NaCl, 4 mM MgCl₂, 1 mM dithiothreitol) with an excess of mant-GTP.

All kinetic measurements were done at 30 °C in a 100 μl reaction volume using 5 nM GEF (Srm1Δ1–27), except for higher concentrations of the mutants with high K_m values that were measured at 20 nM GEF. Data were collected in a Synergy H1 plate reader from BioTek, using Corning 3686 96-well half-area non-binding surface plates. For low concentrations of *Gsp1*–GDP, the time-course data were fit to a combination of two exponential decays. The kinetic parameters of the nucleotide exchange were determined by fitting a Michaelis–Menten equation to an average of 38 data points (ranging from 17 to 91) per *Gsp1* point mutant for a range of substrate concentrations from $[Gsp1\text{-GDP}] = 0.25 \mu\text{M}$ to $[Gsp1\text{-GDP}] \gg K_m$. Michaelis–Menten fits are shown in Supplementary Fig. 4. Michaelis–Menten k_{cat} and K_m parameters for GEF-mediated nucleotide exchange are provided in Supplementary Table 7. For more details on the kinetic analysis, see Supplementary Discussion, Supplementary Methods.

Reporting summary

Further information on research design is available in the Nature Research Reporting Summary linked to this paper.

Data availability

The mass spectrometry proteomics data have been deposited to the PRIDE proteomics data repository with the dataset identifier PXD016338 and are available as Supplementary Tables. Raw biophysics data (cycle kinetics, circular dichroism spectroscopy and NMR), and E-MAPS-scores, scaled SGA scores and their correlations are available from https://github.com/tinaperica/Gsp1_manuscript/tree/master/Data. All other data that support the findings of this study are available within the paper and its supplementary files. Source data are provided with this paper.

Code availability

Custom written R and Python scripts are available without restrictions at https://github.com/tinaperica/Gsp1_manuscript.

21. Levy, E. D. A simple definition of structural regions in proteins and its use in analyzing interface evolution. *J. Mol. Biol.* **403**, 660–670 (2010).
22. Rojas, A. M., Fuentes, G., Rausell, A. & Valencia, A. The Ras protein superfamily: evolutionary tree and role of conserved amino acids. *J. Cell Biol.* **196**, 189–201 (2012).
23. Collins, S. R., Roguev, A. & Krogan, N. J. Quantitative genetic interaction mapping using the E-MAP approach. *Methods Enzymol.* **470**, 205–231 (2010).
24. Schuldiner, M. et al. Exploration of the function and organization of the yeast early secretory pathway through an epistatic miniaarray profile. *Cell* **123**, 507–519 (2005).
25. Giaever, G. et al. Functional profiling of the *Saccharomyces cerevisiae* genome. *Nature* **418**, 387–391 (2002).
26. Collins, S. R. et al. Functional dissection of protein complexes involved in yeast chromosome biology using a genetic interaction map. *Nature* **446**, 806–810 (2007).
27. Cherry, J. M. et al. SGD: *Saccharomyces Genome Database*. *Nucleic Acids Res.* **26**, 73–79 (1998).
28. Benjamini, Y. & Hochberg, Y. Controlling the false discovery rate—a practical and powerful approach to multiple testing. *J. R. Stat. Soc. B* **57**, 289–300 (1995).
29. Benjamini, Y. & Yekutieli, D. The control of the false discovery rate in multiple testing under dependency. *Ann. Stat.* **29**, 1165–1188, 1124 (2001).
30. Jäger, S. et al. Global landscape of HIV–human protein complexes. *Nature* **481**, 365–370 (2011).
31. Jäger, S. et al. Purification and characterization of HIV–human protein complexes. *Methods* **53**, 13–19 (2011).
32. Cox, J. & Mann, M. MaxQuant enables high peptide identification rates, individualized p.p.b.-range mass accuracies and proteome-wide protein quantification. *Nat. Biotechnol.* **26**, 1367–1372 (2008).
33. Cox, J. et al. Accurate proteome-wide label-free quantification by delayed normalization and maximal peptide ratio extraction, termed MaxLFQ. *Mol. Cell. Proteomics* **13**, 2513–2526 (2014).
34. Teo, G. et al. SAINTexpress: improvements and additional features in Significance Analysis of INTeractome software. *J. Proteomics* **100**, 37–43 (2014).
35. Choi, M. et al. MSstats: an R package for statistical analysis of quantitative mass spectrometry-based proteomic experiments. *Bioinformatics* **30**, 2524–2526 (2014).
36. Studier, F. W. Protein production by auto-induction in high density shaking cultures. *Protein Expression Purif.* **41**, 207–234 (2005).
37. Markley, J. L. et al. Recommendations for the presentation of NMR structures of proteins and nucleic acids—IUPAC–IUBMB–IUPAB Inter-Union Task Group on the Standardization of Data Bases of Protein and Nucleic Acid Structures Determined by NMR Spectroscopy. *J. Biomol. NMR* **12**, 1–23 (1998).
38. Mishra, A. K. & Lambright, D. G. High-throughput assay for profiling the substrate specificity of Rab GTPase-activating proteins. *Methods Mol. Biol.* **1298**, 47–60 (2015).
39. Goudar, C. T., Sonnad, J. R. & Duggleby, R. G. Parameter estimation using a direct solution of the integrated Michaelis–Menten equation. *Biochim. Biophys. Acta* **1429**, 377–383 (1999).
40. Malaby, A. W. et al. Methods for analysis of size-exclusion chromatography–small-angle X-ray scattering and reconstruction of protein scattering. *J. Appl. Crystallogr.* **48**, 1102–1113 (2015).
41. Klebe, C., Bischoff, F. R., Ponstingl, H. & Wittinghofer, A. Interaction of the nuclear GTP-binding protein Ran with its regulatory proteins RCC1 and RanGAP1. *Biochemistry* **34**, 639–647 (1995).

Acknowledgements We thank R. Ordonez for contributions to the design of mutations; C. Melero, D. Jeon, S. Mathur, R. D. Kim and K. Kundert for technical help; M. Jaime Garza for contributions to the conformational analysis by NMR; C. Ryan for advice on E-MAP analysis; and D. Agard, G. Narlikar, J. Fraser and J. M. Thornton for discussions. This work was supported by a grant from the National Institutes of Health (R01-GM117189) to T.K. and a Sir Henry Wellcome Postdoctoral Fellowship (101614/Z/13/Z) to T.P. C.J.P.M. is a UCSF Discovery Fellow. T.K. is a Chan Zuckerberg Biohub investigator.

Author contributions T.P., C.J.P.M., N.J.K. and T.K. identified and developed the core questions. T.P. and C.J.P.M. performed the majority of the experiments and data analysis. J.X. and T.P. performed the E-MAP screens. G.M.J. performed the pull-down experiments. D.L.S. and R.K. performed the mass spectrometry experiments and together with T.P. analysed the data. N.O. contributed to the design of *Gsp1* mutants. H.B. contributed to E-MAP analysis. M.J.S.K. suggested the NMR studies. C.J.P.M. and M.J.S.K. performed the NMR experiments and analysed the data. T.P. performed the kinetics experiments. D.G.L. contributed to the analysis of the kinetics data. T.P., C.J.P.M. and Y.Z. purified the proteins. Y.Z. performed the western blot experiments. T.P., C.J.P.M. and T.K. wrote the manuscript with contributions from the other authors. N.J.K. and T.K. oversaw the project.

Competing interests The authors declare no competing interests.

Additional information

Supplementary information The online version contains supplementary material available at <https://doi.org/10.1038/s41586-021-03982-6>.

Correspondence and requests for materials should be addressed to Nevan J. Krogan or Tanja Kortemme.

Peer review information *Nature* thanks Katrin Rittinger and the other, anonymous, reviewer(s) for their contribution to the peer review of this work.

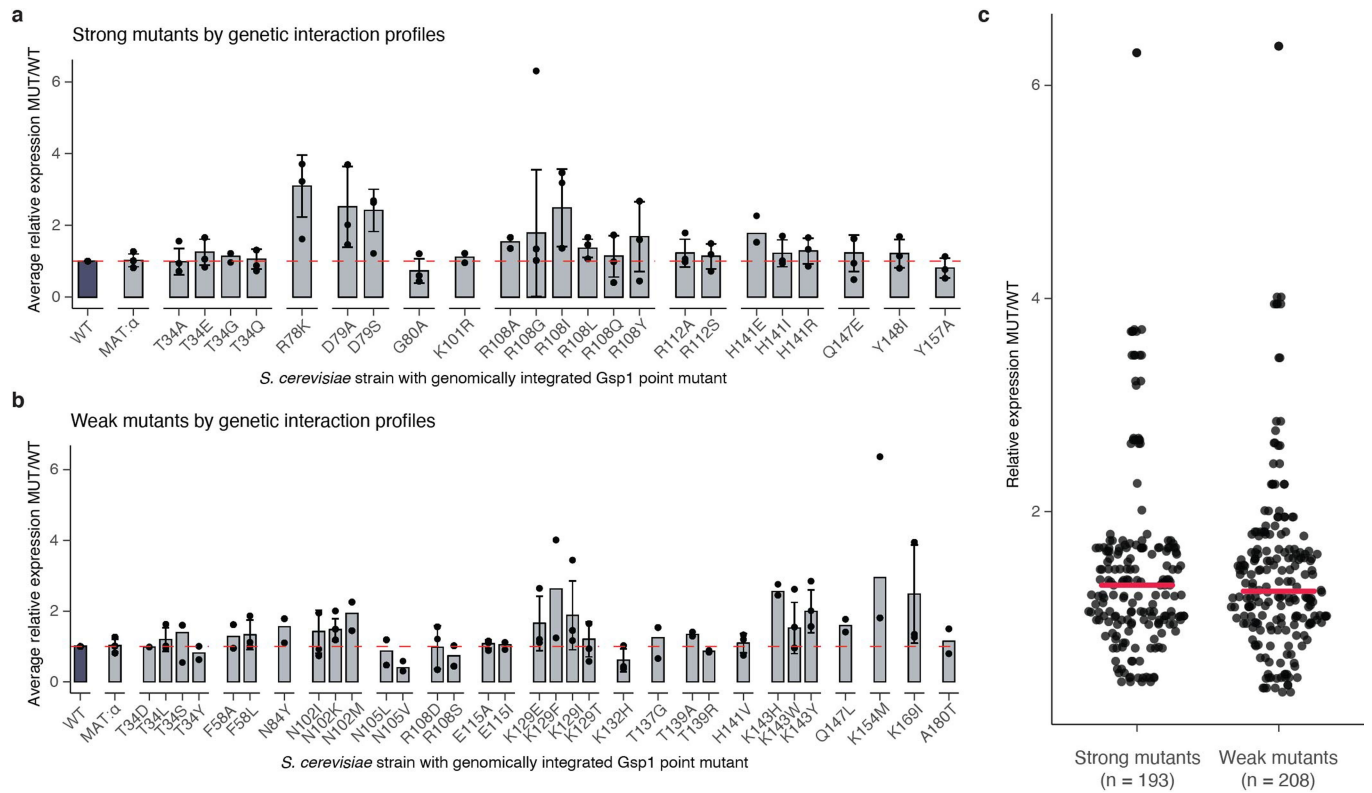
Reprints and permissions information is available at <http://www.nature.com/reprints>.

Article

Extended Data Fig. 1 | Design of interface point mutations in *S. cerevisiae*

Gsp1. Interface residues are categorized as interface core, rim, and support positions (see Supplementary Methods) and provided in Supplementary Table 2. **a–f.** Structures of RAN (Gsp1) in partner-bound conformations with interface residues coloured by partner protein. All mutated Gsp1 residues are shown as spheres.: **a**, Srm1 (GEF) interface core (dark teal) and interface rim and support (light teal) PDB 1I2M; **b**, Rna1 (GAP) interface core (dark orange) and interface rim and support (light orange) PDB 1K5D; **c**, Ntf2 interface core (dark purple) and interface rim and support (light purple) PDB 1A2K; **d**, Residues that are in both the core of the Yrb1 and Yrb2 interfaces (dark yellow), and in only one

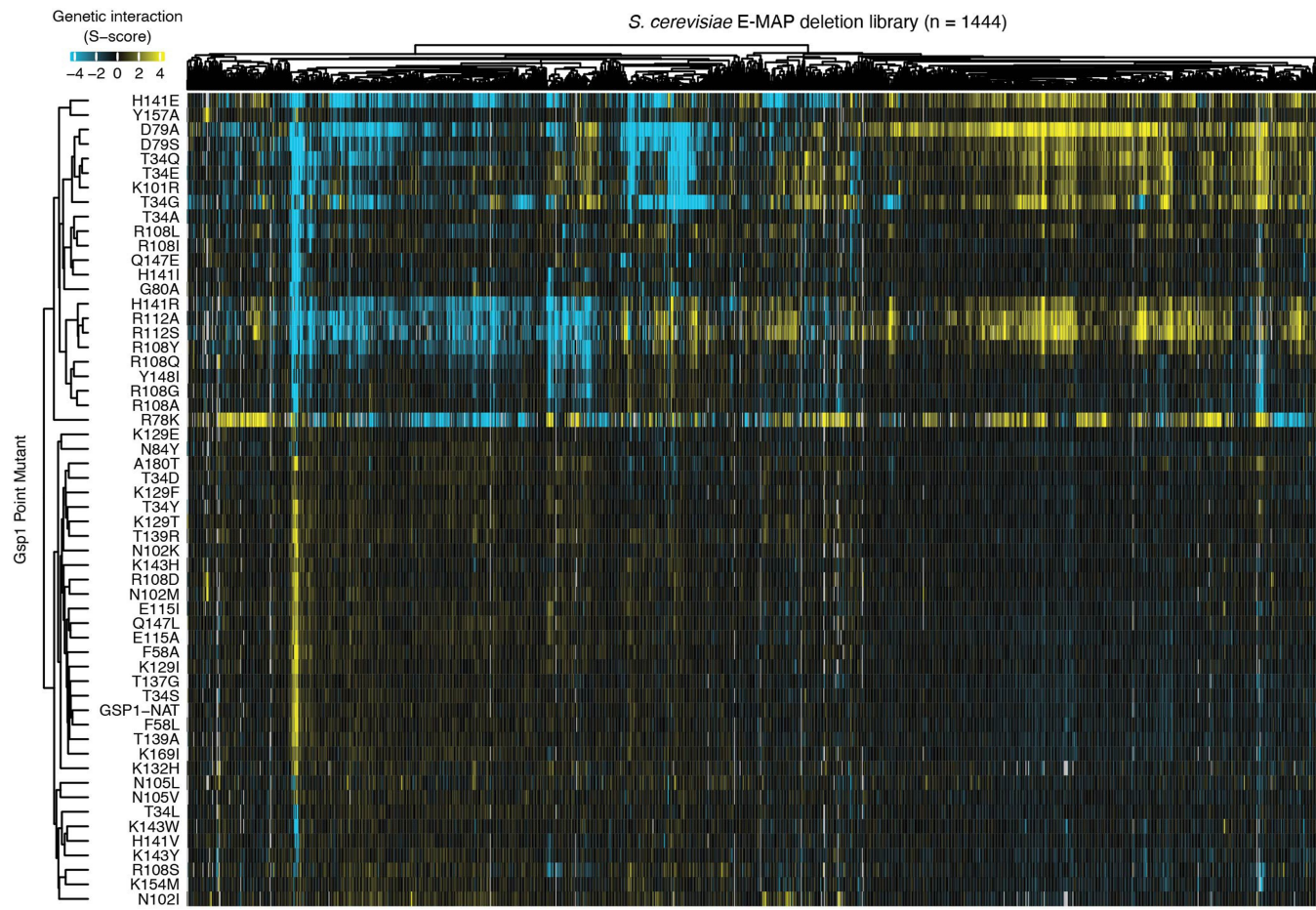
of the two interfaces (light yellow) PDB 1K5D; **e**, Srp1 interface core (dark pink) and interface rim and support (light pink) PDB 1WA5; **f**, Residues that are in the core of four or more (dark green), two to three (green) and one (light green) karyopherin interface. Karyopherins are: Kap95, Crm1, Los1, Kap104, Msn5, Cse1, Mtr10. PDB 2BKU. **g.** Location of Gsp1 residues in partner interfaces. Residues within 5 Å of the nucleotide, in the canonical P-loop, or in the switch I or II regions²² were not mutated. Residues belonging to the switch I, switch II, and C-terminal α helix are indicated by dark navy bars. Chosen Gsp1 point mutation substitutions are provided in Supplementary Table 3.



Extended Data Fig. 2 | Endogenous expression levels of Gsp1 in *S. cerevisiae* strains with genetically integrated *GSP1* point mutations profiled by western blot. **a**, Expression data for strong mutants, defined as mutants with nine or more significant GIs. **b**, Expression data for weak mutants, defined as mutants with fewer than nine significant GIs. In **a**, and **b**, bar heights indicate averages over two or more biological replicates (n) grown on separate days (except for T34D which has only one biological replicate), with error bars indicating one standard deviation for n >= 3. Overlaid points indicate individual biological replicates (each an average over at least 12 technical replicates per

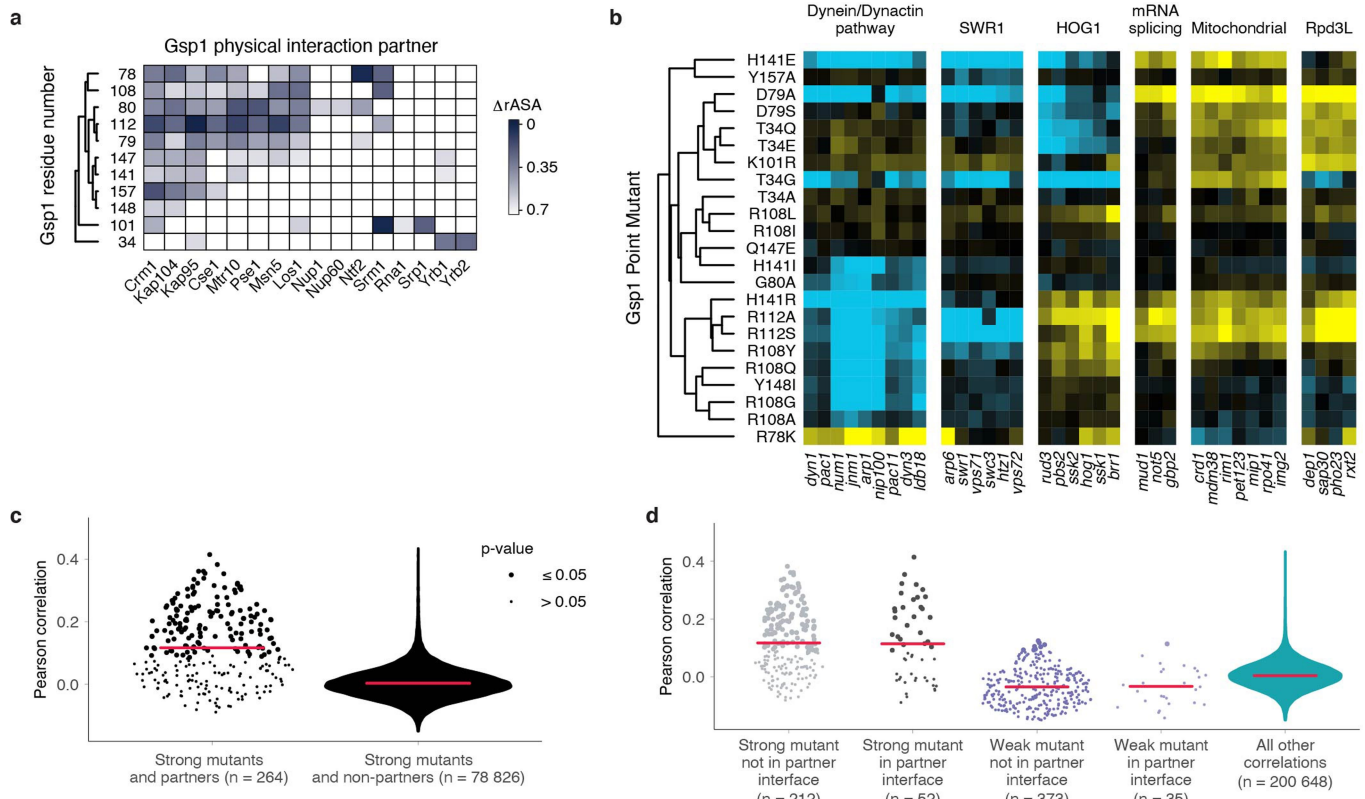
biological replicate for wild-type and MAT: α strains, and between one and six technical replicates per biological replicate for mutant strains). Expression levels are relative to the expression levels of wild-type Gsp1 protein with clonNAT resistance marker (WT) shown as red dashed lines (relative expression of 1). MAT: α is the starting *S. cerevisiae* strain (see Supplementary Methods). **c**, Distributions of average relative expression levels for strong and weak mutants. Each point is as in **a** and **b**. Horizontal pink bars indicate the mean of the point distributions.

Article



Extended Data Fig. 3 | GI profiles of the 56 *GSP1* strains (wild-type *GSP1* with clonNAT cassette and 55 point mutants). Negative S-score (blue) represents synthetic sick or synthetic lethal GIs, positive S-score (yellow) represents suppressive or epistatic GIs; neutral S-scores (no significant GI) are shown in

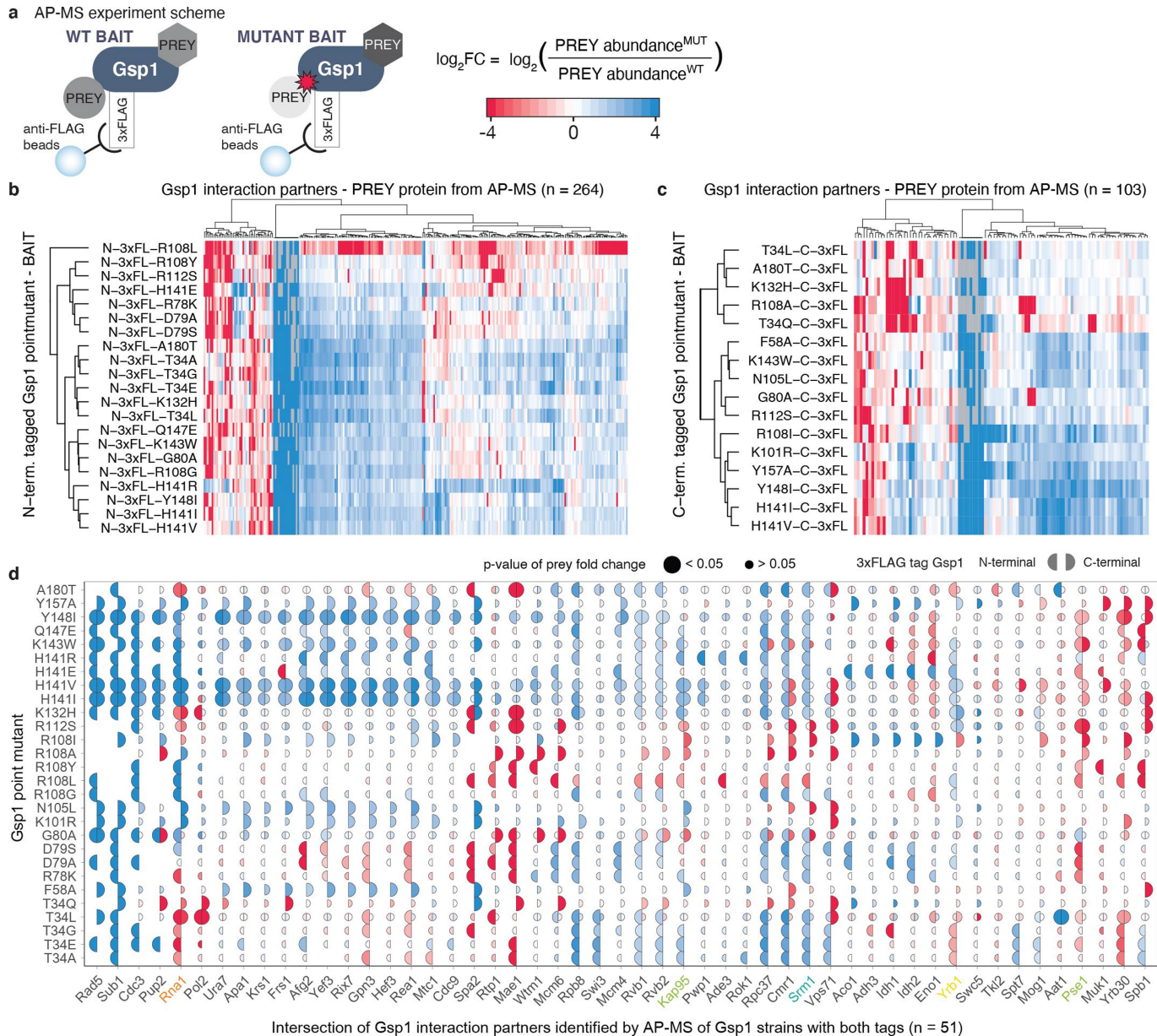
black. Gsp1 point mutants and *S. cerevisiae* genes are hierarchically clustered by Pearson correlation. *GSP1* mutants fall into two clusters: a cluster of 23 strong mutants with nine or more significant GIs and 32 weak mutants with fewer than nine significant GIs.



Extended Data Fig. 4 | Functional profiles of *GSP1* mutants cannot be explained solely by the positions of mutations in interfaces. **a**, Locations of mutated residues in structurally characterized interfaces. $\Delta rASA$ is the difference in accessible surface area of a residue upon binding, relative to an empirical maximum for the solvent accessible surface area of each amino acid residue type (see Supplementary Methods). **b**, GI profiles of *GSP1* mutants group *S. cerevisiae* genes by biological processes and complexes, such as the dynein/dynactin pathway, SWR1 complex, the Hog1 signalling pathway, mRNA splicing, mitochondrial proteins, and the Rpd3L histone deacetylase complex. **c**, Distributions of Pearson correlations between the GI profiles of strong *GSP1* mutants and alleles of *Gsp1* direct interaction partners with available

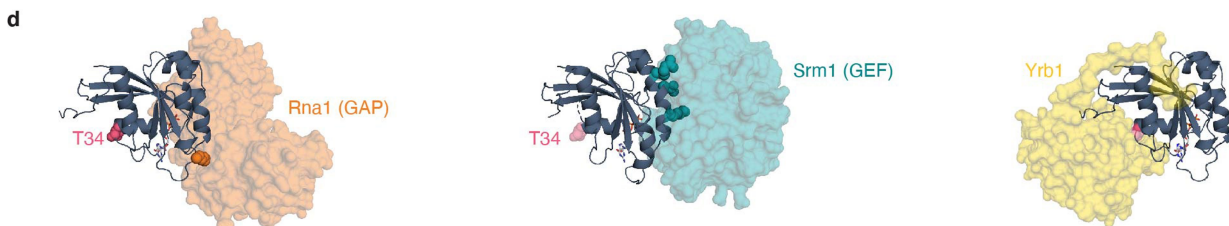
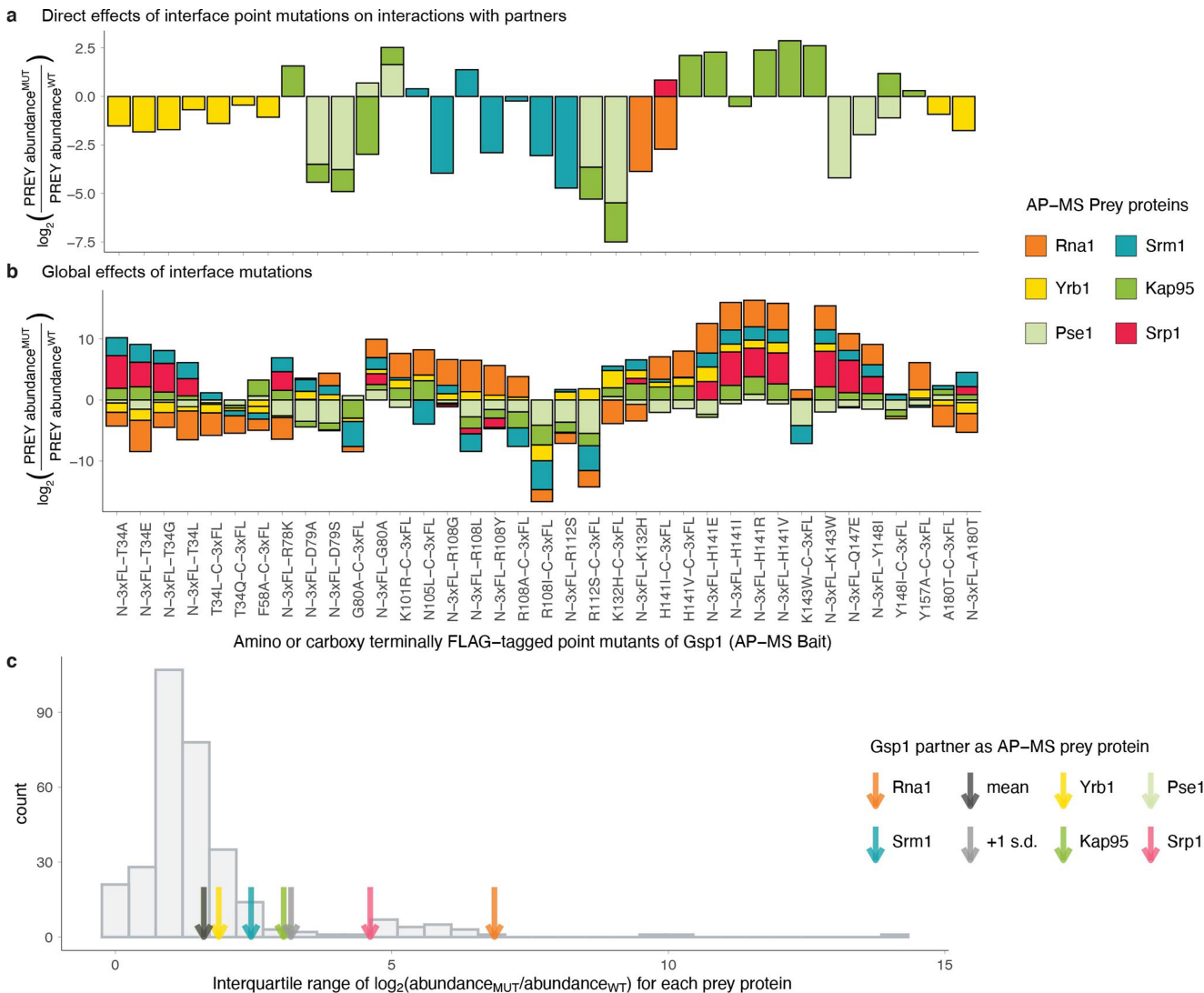
co-complex crystal structures (left) and strong *GSP1* mutants and alleles of all other *S. cerevisiae* genes (right). **d**, Distributions of Pearson correlations between the GI profiles of *Gsp1* interaction partners and strong and weak *GSP1* mutants if mutation is (black and light purple) or is not (grey and dark purple) in the interface with that partner. Teal violin plot on the right represents the distribution of all other Pearson correlations between *GSP1* mutants and *S. cerevisiae* genes. In **c** and **d**, point size indicates the false discovery rate adjusted one-sided (positive) p-value of Pearson correlation, and pink bars indicate the mean of the point distributions; n denotes the number of *GSP1* point mutant-gene GI profile correlations in each category. Data for strong mutants are also shown in Fig. 1e and included here for comparison.

Article



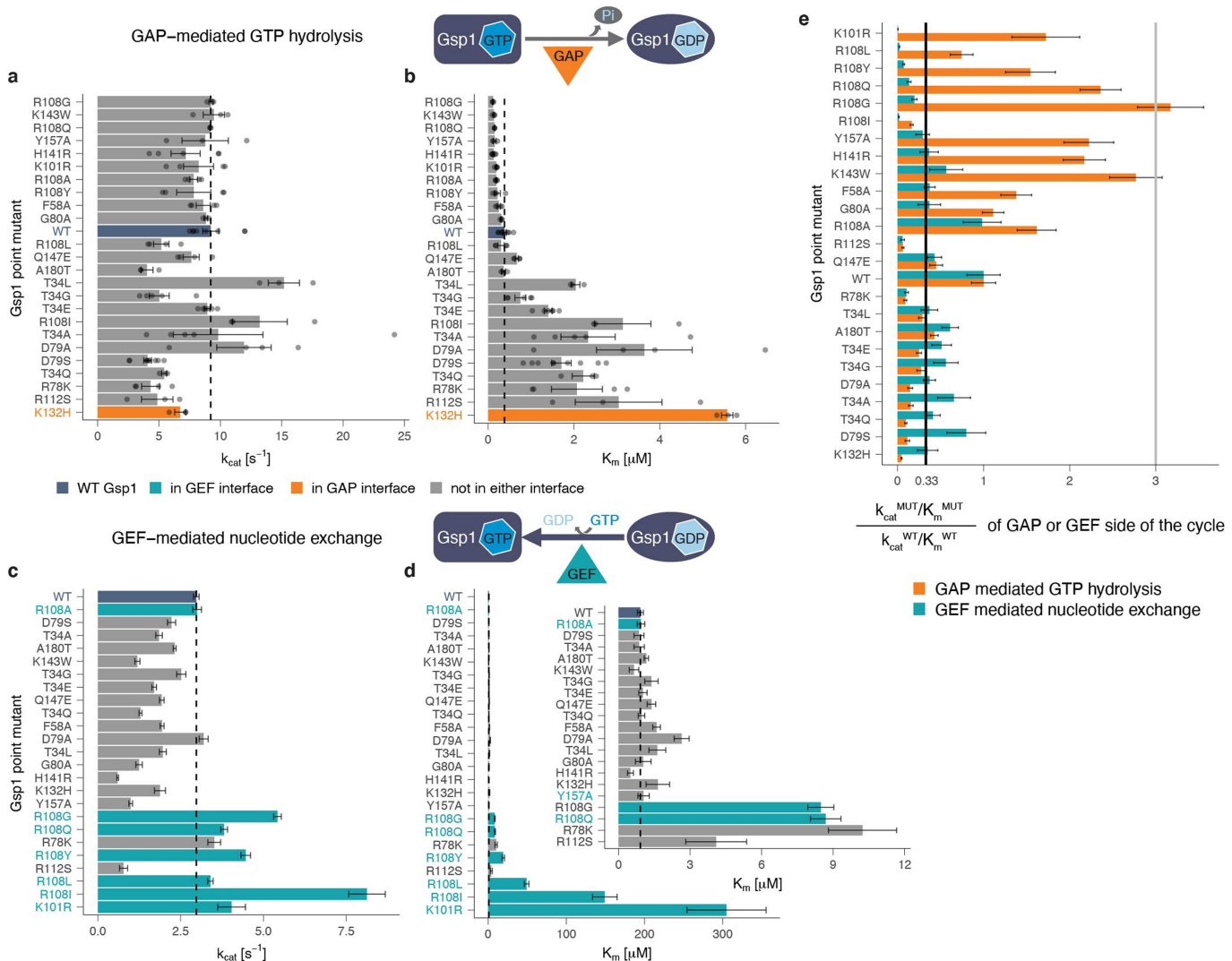
Extended Data Fig. 5 | Interface point mutations in Gsp1 rewire its physical interaction network. **a**, Schematic representation of the affinity purification mass spectrometry (AP-MS) experiment to determine the abundance of pulled-down protein interaction partners of wild type and mutant Gsp1. The change in abundance of partner proteins pulled down with Gsp1 mutants in **b, c**, and **d** is represented as \log_2 -transformed fold change (FC) between abundance of a partner pulled-down with a Gsp1 mutant versus pulled-down with wild-type Gsp1 ($\log_2(\text{abundance(PREY)}^{\text{MUT}}/\text{abundance(PREY)}^{\text{WT}})$). To account for possible tag effects, the fold change in prey abundance was always computed relative to the wild-type protein with the corresponding tag. Decreased abundance compared to pull-down with wild-type Gsp1 is annotated in red and increased abundance in blue. The \log_2 -transformed fold change values are capped at ± 4 . **b**, Amino- and **c**, carboxy terminally 3xFLAG-tagged Gsp1 point mutants (rows) and prey proteins identified by AP-MS (columns) hierarchically

clustered by the \log_2 -transformed fold change in prey abundance. **d**, Prey proteins pulled down by both amino- and carboxy-terminal tagged constructs. Left semi-circle represents an amino-terminal 3xFLAG-tagged Gsp1 point mutant, and right semi-circle represents carboxy-terminal 3xFLAG-tagged Gsp1 point mutant. Semi-circle size is proportional to the significance of the \log_2 -transformed fold change (false discovery rate adjusted p-value) of the prey abundance in pulled-down complexes with a Gsp1 mutant compared to complexes with the wild-type Gsp1. Overall we identified 316 high-confidence prey partner proteins, with the amino- and carboxy-terminally tagged Gsp1 mutants pulling down 264 and 103 preys, respectively, including 51 overlapping preys. The difference in preys identified by experiments with N- or C-terminal tags illustrates the sensitivity of the interaction network to perturbation of Gsp1.



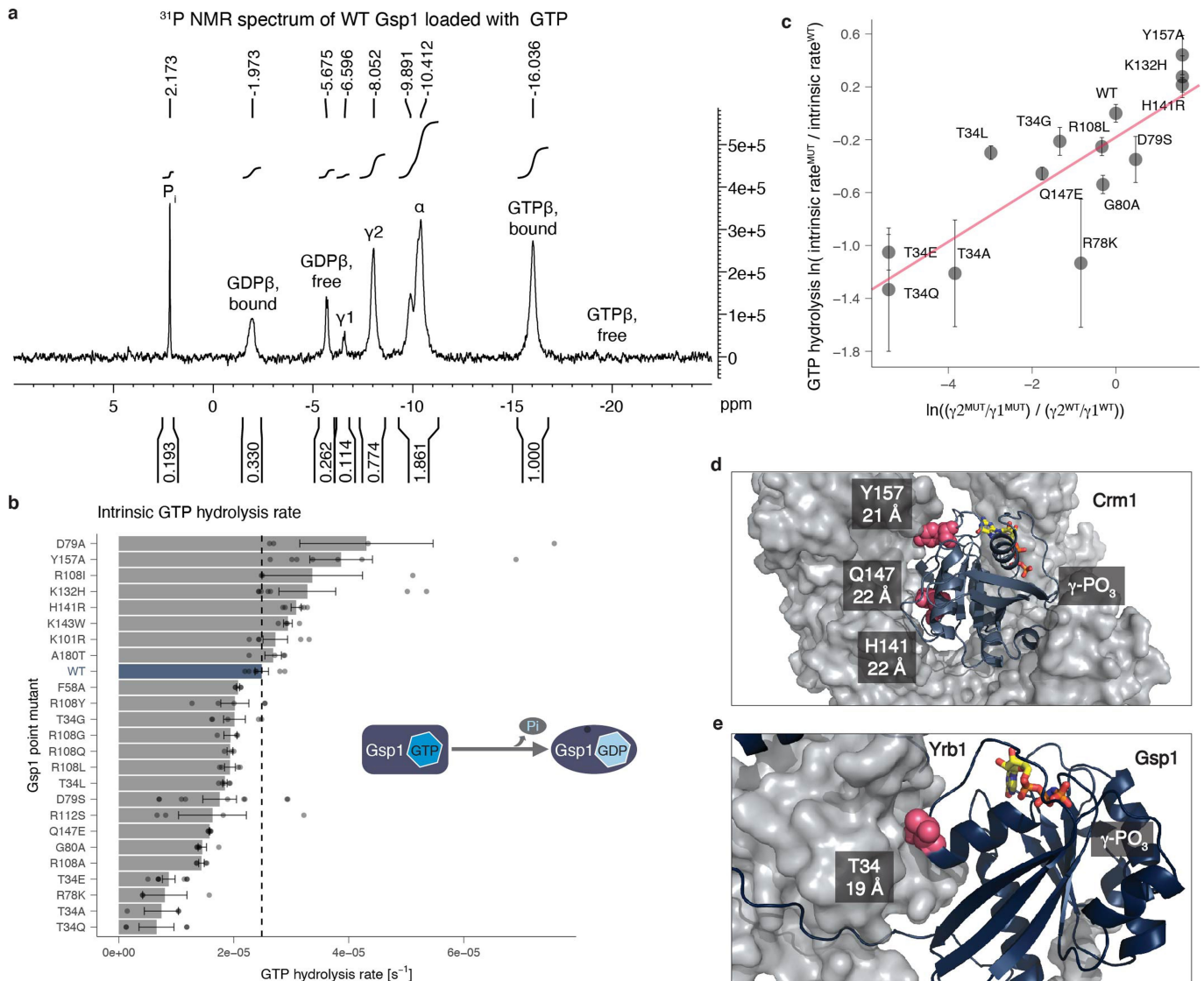
Extended Data Fig. 6 | Gsp1 interface mutations rewire interactions with the core regulators Srm1 and Rna1. **a, b**, Protein-protein interactions between interface mutants of Gsp1 and Gsp1 partners for which there are co-complex X-ray crystal structures (core regulators Srm1 and Rna1, and effectors Yrb1, Kap95, Pse1, and Srp1). Change in pulled-down prey partner abundance is expressed as $\log_2(\text{PREY abundance}_{\text{MUT}}/\text{PREY abundance}_{\text{WT}})$. N-3xFL and C-3xFL labelled mutants are tagged with an amino- or carboxy-terminal triple FLAG tag, respectively, and partners are coloured as indicated. **a**, Bar plot depicting changes in pulled-down prey partner abundance when the point mutation is in the core of the Gsp1 interface with the prey partner. **b**, Bar plot depicting all changes in pulled-down prey partner abundance for core regulators Srm1 and Rna1, and effectors Yrb1, Kap95, Pse1, and Srp1, regardless whether the mutation is directly in the interface core with the partner or not. **c**, Distribution showing the variation in \log_2 -transformed fold change in abundance of all prey proteins pulled down with the Gsp1

mutants, as defined by interquartile range (IQR) across mutants. Values for core partners shown as arrows (Rna1 orange, Srm1 teal, Yrb1 yellow, Kap95 green, Pse1 light green, Srp1 pink). Mean and +1 standard deviation of IQR values are highlighted with a dark grey and a light grey arrow, respectively. The extent to which the abundance of the two cycle regulators Rna1 and Srm1 changed across the Gsp1 point mutants is larger than the change for an average prey protein. All IQR values are provided in Supplementary Table 5. **d**, Position of T34 with respect to the interfaces with Rna1 (GAP, orange surface, PDB 1K5D), Srm1 (GEF, teal surface, PDB 2I1M), and Yrb1 (yellow surface, PDB 1K5D). As the coordinates for T34 are not resolved in the 2I1M structure, in all three structures the pink spheres show the residue location in the aligned 1K5D structure. Gsp1: navy cartoon; GTP nucleotide: stick representation. Residues that were mutated in the Rna1 and Srm1 interfaces are shown in sphere representation and are coloured in orange (Rna1, left) or teal (Srm1, middle).



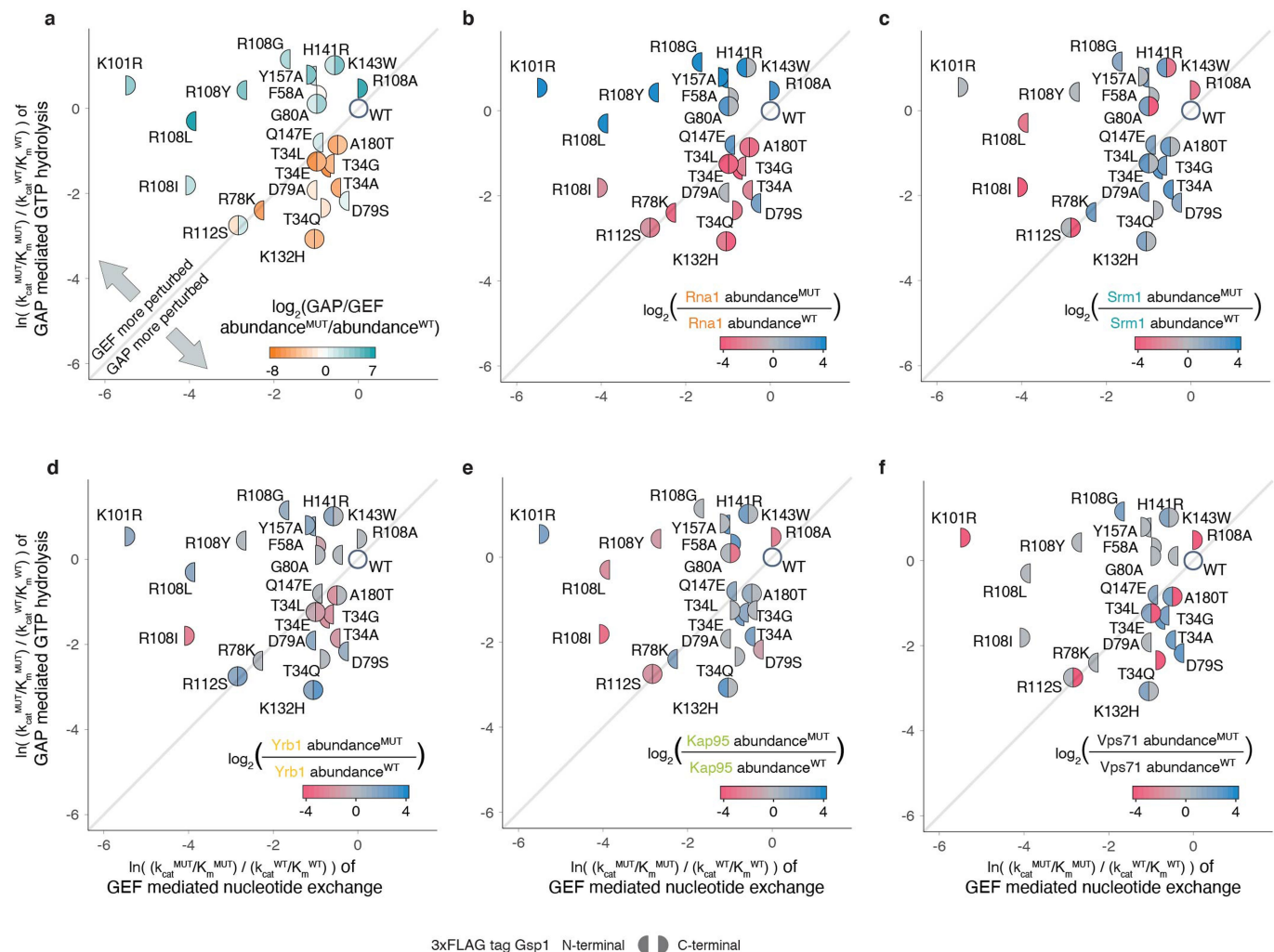
Extended Data Fig. 7 | Effect of Gsp1 point mutations on the in vitro efficiency of GAP-mediated GTP hydrolysis and GEF-mediated nucleotide exchange. **a, b**, k_{cat} and K_m values of GAP-mediated GTP hydrolysis of wild-type and point mutant Gsp1. Error bars represent the standard deviation of the k_{cat} and the K_m parameters from the integrated Michaelis-Menten fit for $n \geq 3$ replicates. **c, d**, k_{cat} and K_m of GEF-mediated nucleotide exchange of wild-type and point mutant Gsp1. Inset shows the K_m bar plot for all but the four mutants with the highest K_m (K101R, R108L, R108I, and R108Y). Error bars represent the value plus/minus the standard error of the Michaelis-Menten fit to data from ≥ 17 measurements at different substrate concentrations. **a, b, c, d**, Dotted lines indicate the wild-type values. Dark blue bar denotes the wild-type Gsp1, and orange and teal bars highlight the residues that are in the core of the interface with the GAP and GEF, respectively. **e**, Comparison of relative change in catalytic efficiencies of GAP-mediated GTP hydrolysis (orange bars) and

GEF-mediated nucleotide exchange (teal bars) defined as $\frac{k_{cat}^{MUT}/K_m^{MUT}}{k_{cat}^{WT}/K_m^{WT}}$. Grey line indicates a three-fold increase compared to wild type and black line indicates a three-fold decrease compared to wild type. Error bars represent the added standard error of the mean (for GAP) or standard error of the fit (for GEF) values of the mutant and the wild-type efficiency (k_{cat}/K_m) values. Mutations not in the interface core with the GAP both increased (3-fold, R108G mutant) and decreased (3 to 10-fold, T34E/Q/A/G, R78K, D79S/A, R108I, and R112S mutants) the catalytic efficiency k_{cat}/K_m of GAP-mediated GTP hydrolysis, compared to wild-type Gsp1. As expected, mutations in the interface core with the GEF (K101, and R108) decreased the catalytic efficiency of GEF-mediated nucleotide exchange >40-fold. However, other mutations not in the GEF interface core (R78K, R112S, Y157A) also decreased the efficiency notably (3- to 10-fold).



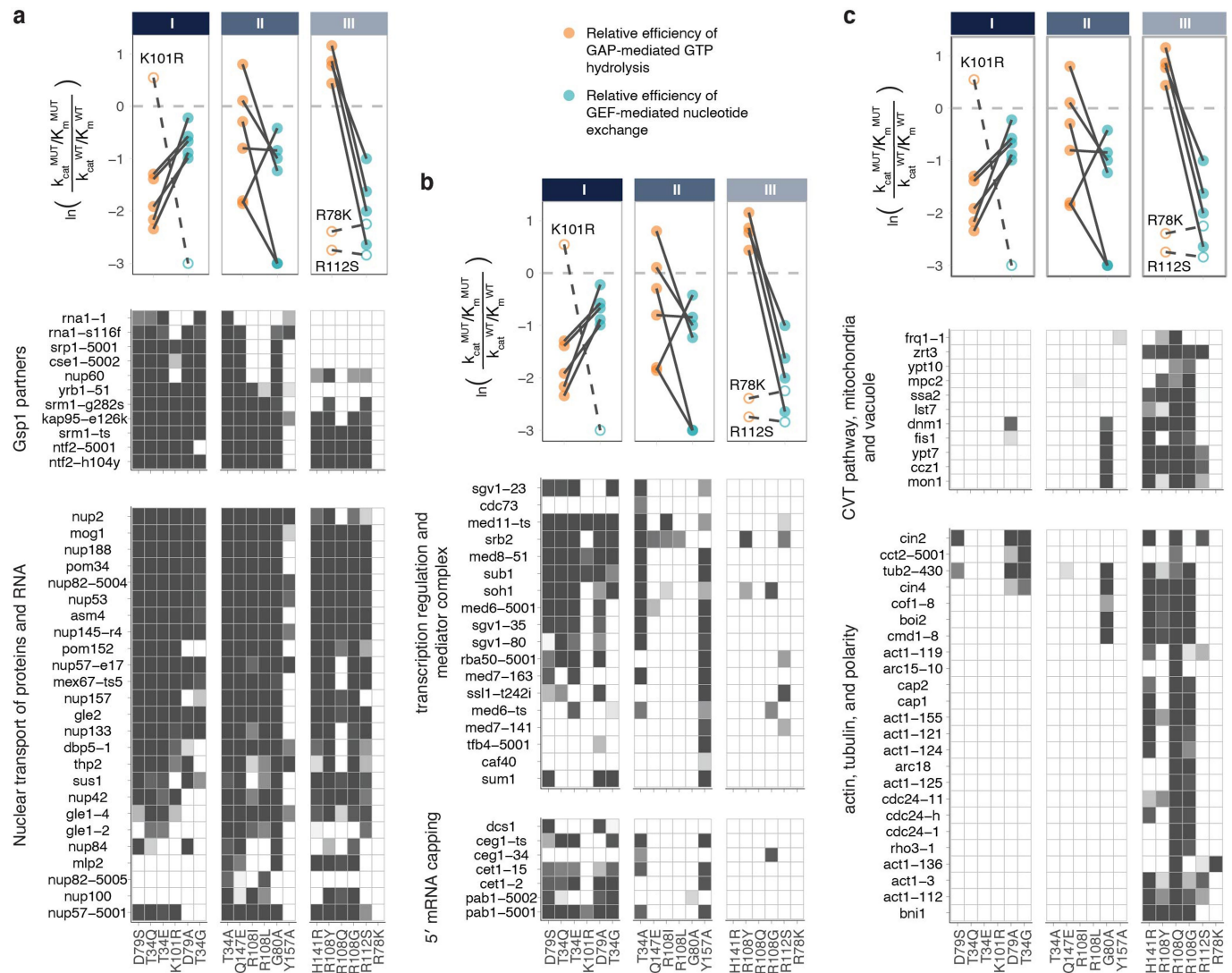
Extended Data Fig. 8 | Gsp1 interface mutations act allosterically to modulate the rate of GTP hydrolysis. **a**, Annotated 1D ³¹P NMR spectrum of wild-type Gsp1 loaded with GTP. Peak areas are computed over intervals shown and normalized to the GTP β bound peak. The peaks from left to right correspond to: free phosphate (P_i), β phosphate of GDP bound to Gsp1 (GDP β bound), β phosphate of free (unbound) GDP (GDP β free), γ phosphate of GTP bound to Gsp1 in conformation 1 (γ_1), γ phosphate of GTP bound to Gsp1 in conformation 2 (γ_2), α phosphate of bound or unbound GDP or GTP, β phosphate of GTP bound to Gsp1 (GTP β bound), β phosphate of free (unbound) GTP (GTP β free). **b**, Rate of intrinsic GTP hydrolysis of wild-type Gsp1 and mutants. Dotted line indicates wild-type value. Error bars represent the

standard deviations from $n \geq 3$ replicates (dots). **c**, Natural log-transformed exchange equilibrium constant between the γ_2 and γ_1 conformations plotted against the relative rate of intrinsic GTP hydrolysis represented as a natural logarithm of the ratio of the rate for the mutant over the rate of the wild type. The pink line is a linear fit. Error bars represent the standard deviation from $n \geq 3$ replicates of intrinsic GTP hydrolysis measurements. **d**, Location of Y157, H141, and Q147 (pink spheres) in the Crm1 interface (grey surface, PDB 3M1I). Gsp1: navy cartoon; GTP nucleotide: yellow stick representation. **e**, Location of T34 (pink spheres) in the interface with Yrb1 (grey surface, PDB 1K5D). Distances from the γ phosphate of GTP to the residue α -carbon are indicated below the residue numbers in **d** and **e**.



Extended Data Fig. 9 | Relative prey protein abundance overlaid onto the effects of each mutation on relative in vitro efficiencies of GAP-mediated GTP hydrolysis and GEF-mediated nucleotide exchange. Relative GAP-mediated hydrolysis and GEF-mediated exchange efficiencies are plotted as $\ln(k_{cat}^{MUT}/K_m^{MUT}) / \ln(k_{cat}^{WT}/K_m^{WT})$. Mutants that affect the efficiency (k_{cat}/K_m) of GEF-catalysed nucleotide exchange more than the efficiency of GAP-catalysed GTP hydrolysis are above the diagonal, and the mutants that affect the GAP-catalysed hydrolysis are below the diagonal. Left semi-circle represents an amino-terminal 3xFLAG-tagged Gsp1 point mutant, and right semi-circle represents a carboxy-terminal 3xFLAG-tagged Gsp1 point mutant, relative to wild-type Gsp1 with the corresponding tag. **a**, Colour represents \log_2 -transformed ratio of GAP and GEF abundance fold change for each Gsp1

point mutant compared to wild type defined as $\log_2((\text{abundance(Rna1)}^{\text{MUT}} / \text{abundance(Rna1)}^{\text{WT}}) / (\text{abundance(Srm1)}^{\text{MUT}} / \text{abundance(Srm1)}^{\text{WT}}))$. Orange coloured mutants pull-down relatively less Rna1 (GAP) and teal mutants less Srm1 (GEF). **b-f**, Colour represents the log-transformed ratio of mutant and wild type pulled-down prey protein represented as $\log_2(\text{PREY abundance}^{\text{MUT}} / \text{PREY abundance}^{\text{WT}})$. Log-transformed relative abundance values are capped at ± 4 . Decreased prey abundance from AP-MS in pulled-down complexes with a mutant Gsp1 compared to complexes with the wild-type Gsp1 is represented in red and increased abundance in blue. Prey proteins: **b**, Rna1 (GAP); **c**, Srm1 (GEF); **d**, Yrb1; **e**, Kap95, and **f**, Vps71. Yrb1 follows a pattern similar to that of Rna1 (GAP), whereas Kap95 and Vps71 are similar to Srm1 (GEF).



point mutants and alleles of *Gsp1* binding partners with available co-complex X-ray crystal structures, and *S. cerevisiae* genes involved in nuclear transport of RNA and proteins. **b**, *GSP1* point mutants and *S. cerevisiae* genes involved in transcription regulation or 5' mRNA capping. **c**, *GSP1* point mutants and *S. cerevisiae* genes involved in the cytoplasm-to-vacuole targeting (CVT) pathway, and actin, tubulin, and cell polarity.

Corresponding author(s): Tanja Kortemme

Last updated by author(s): August 11, 2021

Reporting Summary

Nature Research wishes to improve the reproducibility of the work that we publish. This form provides structure for consistency and transparency in reporting. For further information on Nature Research policies, see [Authors & Referees](#) and the [Editorial Policy Checklist](#).

Statistics

For all statistical analyses, confirm that the following items are present in the figure legend, table legend, main text, or Methods section.

n/a Confirmed

- The exact sample size (n) for each experimental group/condition, given as a discrete number and unit of measurement
- A statement on whether measurements were taken from distinct samples or whether the same sample was measured repeatedly
- The statistical test(s) used AND whether they are one- or two-sided
Only common tests should be described solely by name; describe more complex techniques in the Methods section.
- A description of all covariates tested
- A description of any assumptions or corrections, such as tests of normality and adjustment for multiple comparisons
- A full description of the statistical parameters including central tendency (e.g. means) or other basic estimates (e.g. regression coefficient) AND variation (e.g. standard deviation) or associated estimates of uncertainty (e.g. confidence intervals)
- For null hypothesis testing, the test statistic (e.g. F , t , r) with confidence intervals, effect sizes, degrees of freedom and P value noted
Give P values as exact values whenever suitable.
- For Bayesian analysis, information on the choice of priors and Markov chain Monte Carlo settings
- For hierarchical and complex designs, identification of the appropriate level for tests and full reporting of outcomes
- Estimates of effect sizes (e.g. Cohen's d , Pearson's r), indicating how they were calculated

Our web collection on [statistics for biologists](#) contains articles on many of the points above.

Software and code

Policy information about [availability of computer code](#)

Data collection

Western blots were scanned and analyzed using Image Lab software on a ChemiDoc MP (BioRad). Mass Spectrometry was performed on a Q-Exactive Plus mass spectrometer (Thermo). In vitro kinetics data were collected on a H1 Synergy plate reader from BioTek, using Gen5 (v. 3.03) software. Circular dichroism data were collected on a JASCO J-710 CD-spectrometer using Spectra Manager software (v. 1.53.01). High pressure liquid chromatography was done on an Agilent Technologies 1200 series, using Agilent ChemStation (Rev B 04.03) software. NMR experiments were performed on a Bruker Avance III 600 MHz NMR spectrometer using the Bruker TopSpin software (version 4.0.3).

Data analysis

Structural analysis of Gsp1 interfaces was done using the bio3d R package and custom code provided at https://github.com/tinaperica/Gsp1_manuscript/tree/master/Scripts/complex_structure_analyses. E-MAP analysis was done using open source HT Colony Grid Analyzer Java program (http://sourceforge.net/project/showfiles.php?group_id=163953) and a MATLAB custom toolbox (http://sourceforge.net/project/showfiles.php?group_id=164376). All other custom written code for downstream E-MAP analysis is provided in the accompanying GitHub repository (https://github.com/tinaperica/Gsp1_manuscript/tree/master/Scripts/E-MAP).
Mass spectrometry data were analyzed using MaxQuant (version 1.5.7.4), SAINTExpress and R package MSstats, and custom code is available from https://github.com/tinaperica/Gsp1_manuscript/tree/master/Scripts/APMS. GAP kinetics data were fit using DELA, a freeware software (v 1.0) from Prof. David Lambright, from University of Massachusetts Medical School. GEF kinetics data were fit using custom code. All custom code for fitting and analysing kinetics data is available from https://github.com/tinaperica/Gsp1_manuscript/tree/master/Scripts/kinetics.

For manuscripts utilizing custom algorithms or software that are central to the research but not yet described in published literature, software must be made available to editors/reviewers. We strongly encourage code deposition in a community repository (e.g. GitHub). See the Nature Research [guidelines for submitting code & software](#) for further information.

Data

Policy information about [availability of data](#)

All manuscripts must include a [data availability statement](#). This statement should provide the following information, where applicable:

- Accession codes, unique identifiers, or web links for publicly available datasets
- A list of figures that have associated raw data
- A description of any restrictions on data availability

The mass spectrometry proteomics data have been deposited to the PRIDE proteomics data repository with the dataset identifier PXD016338 and are available as supplementary tables. All other data that support the findings of this study are available within the paper and its Supplementary Files. Additional raw biophysics data (kinetics, CD, and NMR), and E-MAP S-scores, scaled CellMap scores, and their correlations are available from https://github.com/tinaperica/Gsp1_manuscript/tree/master/Data.

Field-specific reporting

Please select the one below that is the best fit for your research. If you are not sure, read the appropriate sections before making your selection.

Life sciences Behavioural & social sciences Ecological, evolutionary & environmental sciences

For a reference copy of the document with all sections, see nature.com/documents/nr-reporting-summary-flat.pdf

Life sciences study design

All studies must disclose on these points even when the disclosure is negative.

Sample size	E-MAP S-scores were determined from 3 to 5 replicates done in independent screens of approximately 25 mutants at the time. Mass spectrometry data were calculated from at least three independent biological replicates (three replicates for each mutant and four, five, and nine replicates for amino-FLAG tagged WT, carboxy-FLAG-tagged WT, and untagged WT, respectively). Each replicate sample culture was grown on a separate day and each sample was injected to a mass spectrometer twice. Western blot expression values represent at least 2 biological replicates, with at least 12 technical replicates per biological replicate for wild type and MAT:α strains, and between one and six technical replicates per biological replicate for mutant strains. GEF-mediated nucleotide exchange kinetics parameters were determined by fitting 17 to 91 data points ranging from 0.25 μM Gsp1 to concentrations approximately 10-fold over the Km value. GAP-mediated GTP hydrolysis kinetic parameters and their standard deviations were calculated from three or more kinetic curves, from two or more independently GTP-loaded protein samples (loaded and run on separate days).
Data exclusions	No data were excluded.
Replication	All experiments yielded consistent results. Precise numbers of repeats for each experiment are provided in figure legends and methods.
Randomization	The combinations of the approximately 25-30 mutants that were screened together in an E-MAP screen were randomised. For all other experiments the samples were not randomized, but appropriate controls were included.
Blinding	No blinding was performed.

Reporting for specific materials, systems and methods

We require information from authors about some types of materials, experimental systems and methods used in many studies. Here, indicate whether each material, system or method listed is relevant to your study. If you are not sure if a list item applies to your research, read the appropriate section before selecting a response.

Materials & experimental systems

n/a	Involved in the study
<input type="checkbox"/>	<input checked="" type="checkbox"/> Antibodies
<input type="checkbox"/>	<input checked="" type="checkbox"/> Eukaryotic cell lines
<input checked="" type="checkbox"/>	<input type="checkbox"/> Palaeontology
<input checked="" type="checkbox"/>	<input type="checkbox"/> Animals and other organisms
<input checked="" type="checkbox"/>	<input type="checkbox"/> Human research participants
<input checked="" type="checkbox"/>	<input type="checkbox"/> Clinical data

Methods

n/a	Involved in the study
<input checked="" type="checkbox"/>	<input type="checkbox"/> ChIP-seq
<input checked="" type="checkbox"/>	<input type="checkbox"/> Flow cytometry
<input checked="" type="checkbox"/>	<input type="checkbox"/> MRI-based neuroimaging

Antibodies

Antibodies used

Rabbit anti-RAN (CAT # PA 1-5783, ThermoFisher Scientific) primary antibody for anti-Gsp1 staining 1:1000
Goat anti-Rabbit-IgG(H+L)-HRP (CAT #31460, Thermo Fisher) secondary antibodies

Validation

Validated by the manufacturer to detect *S. cerevisiae* Gsp1 in Western blot
Validated by the manufacturer for a range of Rabbit IgG

Eukaryotic cell lines

Policy information about [cell lines](#)

Cell line source(s)

The starting *S. cerevisiae* strain used was: MAT: α his3D1; leu2D0; ura3D0; LYS2 β ; can1::STE2pr-SpHIS5 (SpHIS5 is the *S. pombe* HIS5 gene); lyp1D::STE3pr-LEU2 (as described in Collins et al, 2010, Meth Enzymol.)

Authentication

The point mutations, as well as clonNAT and 3xFLAG insertions into the Gsp1 genomic region were confirmed by PCR and standard sequencing.

Mycoplasma contamination

Cells were not tested for mycoplasma contamination.

Commonly misidentified lines
(See [ICLAC](#) register)

No commonly misidentified cell lines were used.